Electronic Supplementary Material (ESI) for Chemical Communications.

Experimental and Supplementary Information for

A Molecular Aluminium Fulleride

Samuel Ray Lawrence,[a,b] Tobias Rüffer,[b] Andreas Stasch,[a]* and Robert Kretschmer[b]*

[a]*EaStCHEM School of Chemistry, University of St Andrews, North Haugh, St Andrews, KY16 9ST, UK*

[b]*Institute of Chemistry, Chemnitz University of Technology, 09111 Chemnitz, Germany.*

1. Experimental Details

1.1. General information

All manipulations were carried out using standard Schlenk and glove box techniques under an atmosphere of high purity dinitrogen. Benzene and toluene were dried and distilled under inert gas over sodium prior to use.

Yields or conversions in solution were determined by integration of ^{1}H NMR spectra against an internal standard (such as added tetramethylsilane(TMS)/C_6D_6 insert). Note that reaction mixtures often afforded dark precipitate during reactions. Thus, not all (^{Dipp}nacnac)Al units contributed to the given solution yields or conversions even though they represented the dominating species in solution. C_{60} was purchased from Alfa Aesar (99%) and stored in a glove box. The syntheses of [(^{Dipp}nacnac)Al][1] and [{(^{Mes}nacnac)Mg}$_2$][2] were performed according to literature procedures.

^{1}H and ^{13}C{^{1}H} NMR spectra were recorded on Bruker Avance III 500 and Avance Neo 600 spectrometers in deuterated benzene or toluene and were referenced to the residual ^{1}H or ^{13}C{^{1}H} resonances of the solvent used. High temperature NMR spectra were recorded on a Bruker DPX 250 MHz. UV/Vis spectra were recorded using a Genesys 6 spectrophotometer in sealable quartz cells. Elemental analyses were performed with a Vario EL Cube (Elementar Analysensysteme GmbH). IR spectra were recorded with a Agilent Cary 630 spectrometer equipped with a diamond ATR unit. MALDI-TOF MS spectra were taken using BRUKER autoflex maX MALDI-TOF instrument and each respective sample was mixed with a matrix (1,8-dihydroxy-9,10-dihydroanthracen-9-one), 1:20 by mass, and then the mixture was pasted onto the plate.

*1.2. Synthesis of [{(^{Dipp}nacnac)Al}$_3$C$_{60}$] (**2**)*

[{(^{Dipp}nacnac)Al] **1** (11.3 mg, 25.4 µmol, 3.00 equiv.) and C_{60} (6.1 mg, 8.46 µmol) were added to an NMR tube with J. Young valve and dissolved in toluene-d_8 (0.6 mL), immediately giving a green-black solution. The mixture was left standing at room temperature and the reaction was followed by ^{1}H NMR spectroscopy at regular intervals. Full consumption of [(^{Dipp}nacnac)Al] **1** was observed after one day, with the ^{1}H NMR spectrum showing only resonances for [{(^{Dipp}nacnac)Al}$_3$C$_{60}$] **2**; conversion of **1**: 100%. Over the following two days, crystals of **2** suitable for X-ray crystallographic analysis formed from the toluene-d_8 solution; Yield: 16.2 mg (75%). ^{1}H NMR (600.1 MHz, toluene-d_8, 298 K) δ = 1.07 (d, J_{HH} = 6.7 Hz, 18H, CH(CH_3)$_2$), 1.09 (d, J_{HH} = 6.9 Hz, 18H, CH(CH_3)$_2$), 1.39 (d, J_{HH} = 6.7 Hz, 18H, CH(CH_3)$_2$), 1.45 (d, J_{HH} =

6.7 Hz, 18H, CH(CH_3)$_2$), 1.66 (s, 18H, NCCH_3), 3.53 (sept, J_{HH} = 6.8 Hz, 6H, CH(CH$_3$)$_2$), 3.63 (sept, J_{HH} = 6.8 Hz, 6H, CH(CH$_3$)$_2$), 4.98 (s, 3H, γ-CH), 6.92 (d, J_{HH} = 1.6 Hz, 3H, ArH), 6.93 (d, J_{HH} = 1.6 Hz, 6H, ArH), 6.97–7.01 (m, 9H, ArH); ^{13}C{^{1}H} NMR (125.8 MHz, toluene-d_8, 298 K) δ = 23.65 (CH(*C*H$_3$)$_2$), 24.03 (overlapping (CH(*C*H$_3$)$_2$) and NC*C*H$_3$), 24.88 (CH(*C*H$_3$)$_2$), 24.94 (CH(*C*H$_3$)$_2$), 29.92 (*C*H(CH$_3$)$_2$), 30.06 (*C*H(CH$_3$)$_2$), 76.31 (Al-*C*$_2$(C$_{60}$)), 97.69 (γ-*C*H), 125.20 (Ar-*C*), 125.37 (Ar-*C*), 129.10 (Ar-*C*), 129.15 (Ar-*C*), 137.79 (*C*$_{60}$), 139.11 (*C*$_{60}$), 139.17 (*C*$_{60}$), 143.72 (Ar-*C*), 143.99 (Ar-*C*), 147.13 (*C*$_{60}$), 150.10 (*C*$_{60}$), 150.65 (*C*$_{60}$), 151.60 (*C*$_{60}$), 155.58 (*C*$_{60}$), 164.04 (Ar-*C*), 172.23 (*C*$_{60}$), 175.02 (N*C*CH$_3$). UV/Vis (toluene) λ_{max} [nm] (ε in mol^{-1}dm^{3}cm^{-1}): 341 (~68,000), 426 (5,919), 468sh (4,493), 632 (2,650), 660sh (2,185). IR ν_{max}/cm^{-1} 2960vs, 2924vs, 2863s, 2529br, 2462w, 2378br, 2177s, 2158s, 2023w, 1994w, 1968w, 1943w, 1526vs, 1462s, 1435s, 1388vs, 1314s, 1256s, 1179s, 1149s, 933s, 876s, 850vs, 797vs, 758vs.

For complex **2**, elemental analysis consistently afforded values 1-5% too low for C that we have attributed to incomplete combustion of materials with high C content. A similar phenomenon has been observed previously when acquiring elemental analysis of [{(^{Dep}nacnac)Mg}$_2$C$_{60}$.[3] Solvent of crystallisation, five toluene molecules per formula unit, was present in the crystal lattice of **2** and made reproducible C,H,N analysis difficult. Calculated: 85.94 C, 6.03 H, 4.09 N; average (from 5 runs): 82.76 C, 6.052 H, 3.44 N; range: 80.87–84.66 C, 5.835–6.383 H, 3.16–3.53 N.

In the MALDI-TOF mass spectrum of **2** isotope patterns of high *m*/*z* peaks were observed (1183 m/z) (see Figure S12). The samples were prepared as 20:1 mixtures of 1,8-dihydroxy-9,10-dihydroanthracen-9-one (Dianthrol):**2**, and these patterns are attributed to decomposition compounds, [{C$_{60}$(O)H$_x$}(Dianthrol)$_2$]. Alternatively, they may be tentatively assigned to [{(^{Dipp}nacnac)Al}C$_{60}$H$_2$O], as a partially hydrolysis product of **2**, although this is unlikely. An almost identical isotope pattern is observed at +15 m/z from this and as such we suspect this to be a similar set of isomers with an additional epoxide functionality on the carbon cage. Additional m/z peaks at 1369 could not be confidently assigned, and no species of higher molecular weight were observed, which is unsurprising given the mounting evidence for the hydrolysis of the sample.

A note on stoichiometry: Reactions in a 2:1 or 1:1 stoichiometric ratio of (^{Dipp}nacnac)Al:C$_{60}$ only forms compound **2** and a stoichiometry greater than 3:1 leaves unreacted [(^{Dipp}nacnac)Al] **1** in solution and full consumption of C$_{60}$ (observed by ^{1}H and ^{13}C{^{1}H} NMR spectroscopy). Sub-stoichiometric addition of [(^{Dipp}nacnac)Al] to C$_{60}$ gives rise to a deep red solution (as opposed

to deep green compound **2**) and the ^{1}H NMR spectrum suggests an intractable mixture of products that could so far not be separated.

A note on solvent choice: Removal of aromatic solvent through applied vacuum or evaporation causes a brown solid to form which is no longer soluble in benzene or toluene. Dissolution of **2** in mixtures of toluene with coordinating solvent, such as THF or acetonitrile, affect an immediate solution colour change, alongside precipitation.

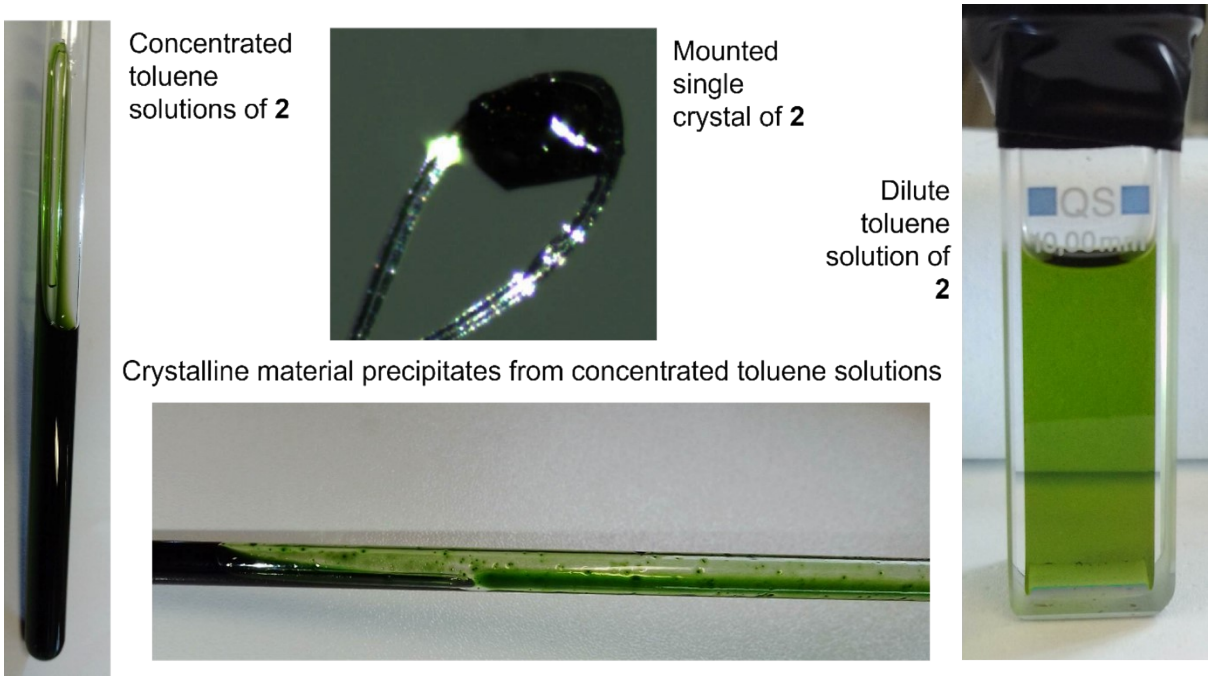

Figure S1: Pictures of concentrated and dilute toluene solutions of **2**, and mounted single crystal of **2**.

1.3 Investigation into the reversibility of {([Dipp]nacnac)Al} coordination to C_{60}: variable temperature NMR spectroscopic studies and attempts to chemically trap [([Dipp]nacnac)Al] at high temperatures

A ^{1}H NMR spectrum of **2** in toluene-d_8 at room temperature was taken, and the spectrometer probe heated to 80 °C. After establishing a stable temperature, a further ^{1}H NMR spectrum, and a ^{13}C{^{1}H} NMR spectrum of the sample were recorded. A comparative ^{1}H NMR spectrum of [([Dipp]nacnac)Al] **1** was also recorded at 80 °C, as a standard.

It was ascertained that **2** is unstable at elevated temperatures for prolonged periods, with a dark-brown solution forming and brown solid precipitating. The high temperature ^{1}H NMR

spectrum shows no resonances that accord with compound **1**, and with only signs of starting decomposition. The $^{13}C\{^{1}H\}$ NMR spectrum was inconclusive, as only resonances associated with toluene were present, despite the number of scans (n > 2000). The ^{1}H NMR spectrum taken after prolonged heating shows an intractable mixture of products with notable fullerene C-H resonances between δ = 5.2–6.0 ppm.

Next, a selection of reagents were employed to chemically trap any transient [(^{Dipp}nacnac)Al] **1** that could be forming at elevated temperatures.

Firstly, to a toluene-d_8 solution of compound **2** was added a large excess of C_6F_6 and the reaction was followed using ^{1}H and $^{19}F\{^{1}H\}$ NMR spectroscopy. No reaction occurs at room temperature but heating the mixture at 50 °C for ten hours lead to the consumption of both C_6F_6 (according to $^{19}F\{^{1}H\}$ NMR spectroscopy) and compound **2** (^{1}H NMR spectroscopy), with concomitant formation of a dark red-brown precipitate. The $^{19}F\{^{1}H\}$ spectrum is absent of any resonances, and the ^{1}H NMR spectrum contains only resonances associated with decomposition products (from prolonged heating). There is no evidence of the formation of [(^{Dipp}nacnac)Al(F)(C_6F_5)] (the intended trapped species).[5]

Hydrogenation of compound **2** occurs at ambient conditions (1 bar H_2, room temperature), but the reaction affords no resonances in the ^{1}H NMR spectrum that accord with those of previously reported ^{Dipp}nacnac-supported aluminium hydride species.[6]

Whilst [(^{Dipp}nacnac)Al] **1** inserts into the C-O bond of THF, giving a cyclic alkoxide derivative[5a], a 1:1 toluene-d_8/THF-d_8 solution of compound **2** instead affects immediate precipitation of two solids of different appearance: a spongy colourless solid suspected to be polytetrahydrofuran, and a dark red insoluble material of unknown composition.

The reaction of **2** with either an alkene (1-hexene) or an alkyne (diphenylacetylene) offered inconclusive results, giving mixtures of products in each respective ^{1}H NMR spectrum. The previously reported metallocyclopropene compound [(^{Dipp}nacnacAl(η^2-C_2Ph_2)] was, however, observed as a minor product in the latter reaction.[7]

These experiments present contrasting reactivity to that of [(^{Dipp}nacnac)Al] **1** and as such are considered a sign that complete reversibility of aluminium coordination to C_{60} is significantly hindered. The appearance of [(^{Dipp}nacnacAl(η^2-C_2Ph_2)] during the reaction of **2** with PhCCPh

does however suggest that Al-C bond scission cannot be ruled out as a possibility at elevated temperatures.

*1.4. H_2O quench of [{(^{Dipp}nacnac)Al}$_3C_{60}$] **2***

A toluene-d_8 solution of [{(^{Dipp}nacnac)Al}$_3C_{60}$] **2** (approx. 7.5 μmol) was prepared as described above and used as is. The concentrated solution of **2** was diluted in a Schlenk flask with toluene (5 mL) and distilled water (0.1 mL) was added with a syringe whilst stirring. An immediate colour change from deep green to orange-red occurred. The solution was stirred for 15 minutes, and then filtered. All volatiles were removed in vacuo, the residue dissolved in 1 mL of toluene, and 5 mL of *n*-hexane layered on top. Once the solvents are mixed, a dark orange-brown precipitate is formed. The solution is filtered off and the solid washed with 3 mL of *n*-hexane and collected. The ^{1}H and ^{13}C{^{1}H} NMR spectra of the residue show characteristic resonances of $C_{60}H_6$.[8] ^{1}H NMR (600.1 MHz, toluene-d_8, 298 K) δ = 5.19 (s, 6H, $C_{60}H_6$). ^{13}C{^{1}H} NMR (150.9 MHz, toluene-d_8, 298 K) δ = 51.86 (C_{60}-H), 142.41, 143.05, 143.10, 133.26, 145.67, 145.75, 145.80, 153.85, 157.96.

MALDI-TOF mass spectrometry was conducted on red-orange samples of $C_{60}H_6$ which was produced from the direct hydrolysis of compound **2**, and the purity confirmed by ^{1}H and ^{13}C NMR spectroscopy. The mass spectrum shows only isotope patterns for C_{60}, despite the notable disparity of physical properties (C_{60} is purple and sparingly soluble in toluene, whilst $C_{60}H_6$ is red-orange and soluble in toluene, which is how the sample was observed).

MALDI-TOF mass spectrometry was performed on compound **2** instead, and provided an isotope pattern very similar to the one previously reported for $C_{60}H_6$ (i.e. seven m/z peaks from 720.43 – 726.53 with a spacing of roughly 1 m/z between each peak; representing $C_{60}H_x$, x = 0–6).[8] Similar patterns of lower intensity are observed at +16 m/z and +32 m/z to this, corresponding to $C_{60}H_xO$ and $C_{60}H_xO_2$ species, respectively. Such fullerane epoxides are known to form when the hydrolysis step of $C_{60}H_6$ preparation is performed in air. The authors of the aforementioned study[8] also observed dehydrogenation of $C_{60}H_6$ arising from thermal decomposition and is it suspected here that dehydrogenation also occurs during the ionisation of $C_{60}H_6$, which explains the observed mixed m/z pattern.

*1.4. Synthesis of [{(^{Mes}nacnac)Mg}$_6C_{60}$] from [{(^{Dipp}nacnac)Al}$_3C_{60}$] **2***

A toluene-d_8 solution of [{(^{Dipp}nacnac)Al}$_3C_{60}$] **2** was prepared as described above and diluted to *ca.* 2.2 mmol dm^{-3} (calculated using a TMS internal standard). To the 0.6 mL (1.34 μmol) toluene-d_8 solution was added [{(^{Mes}nacanc)Mg}$_2$] (3.0 mg, 4.19 μmol, 3.12 equiv.) and the

mixture was heated at 80 °C for one hour. During this time, the deep green colour of **2** dissipates and a dark brown/yellow colour persists. Resonances in the ^{1}H NMR spectrum show one major product with almost identical ppm values to those of [{(^{Mes}nacnac)Mg}$_6$C$_{60}$] in deuterated benzene.[3] [{(^{Mes}nacnac)Mg}$_6$C$_{60}$] was later prepared independently and its ^{1}H and ^{13}C{^{1}H} NMR spectra confirmed the identity of the dominant species. ^{1}H NMR (600.1 MHz, toluene-d_8, 298 K) δ = 1.69 (s, 36H; NCCH_3), 2.28 (s, 72H; *o*-CH_3), 2.51 (s, 36H; *p*-CH_3), 4.94 (s, 6H; γ-C*H*), 6.96 (s, 24H; Ar-*H*); ^{13}C{^{1}H} NMR (150.9 MHz, toluene-d_8, 298 K) δ = 20.0 (NC*C*H$_3$), 22.1 (*p*-*C*H$_3$), 23.9 (*o*-*C*H$_3$), 95.9 (γ-*C*H), 130.3 (Ar-*C*), 132.0 (Ar-*C*), 134.2 (Ar-*C*), 144.7 (Ar-*C*), 153.3 (C_{60}), 170.1 (N*C*CH$_3$).

2. NMR, IR, and UV-vis spectra

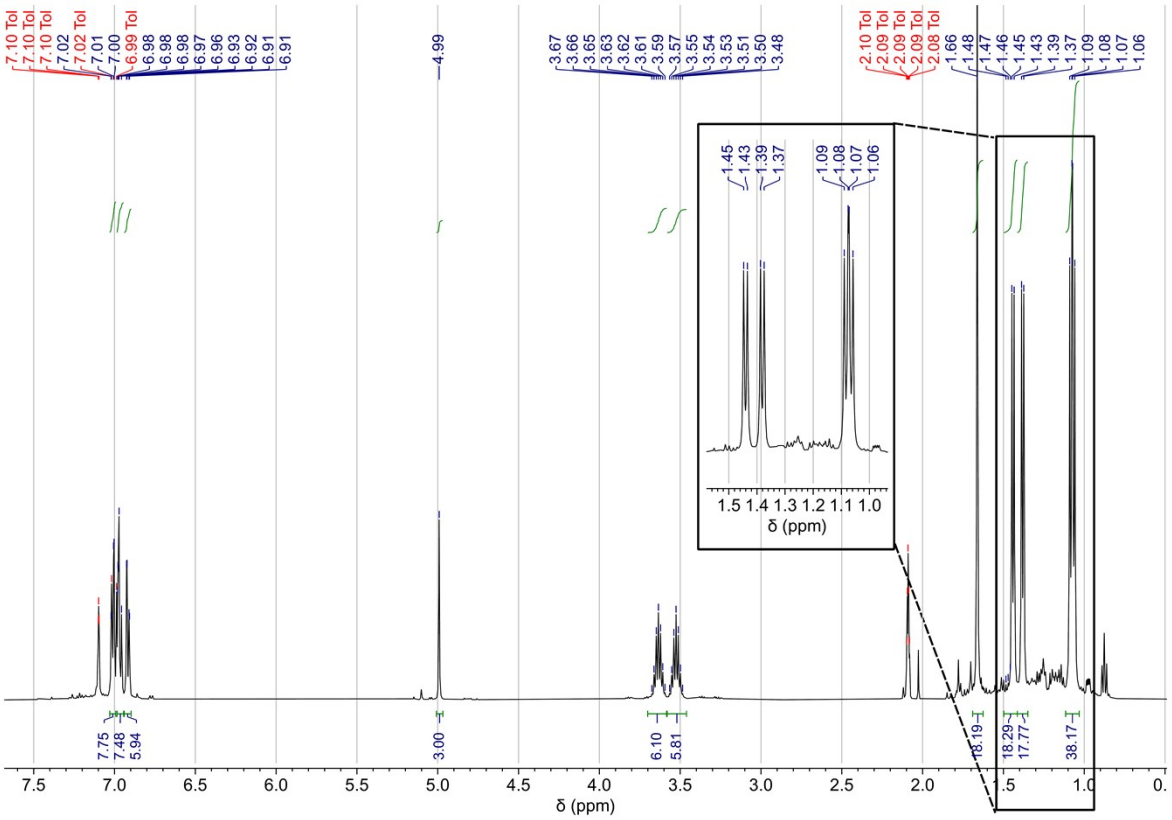

Figure S2: ^{1}H NMR spectrum (500.3 MHz, 298 K) of a crude reaction mixture of **2** in toluene-d_8.

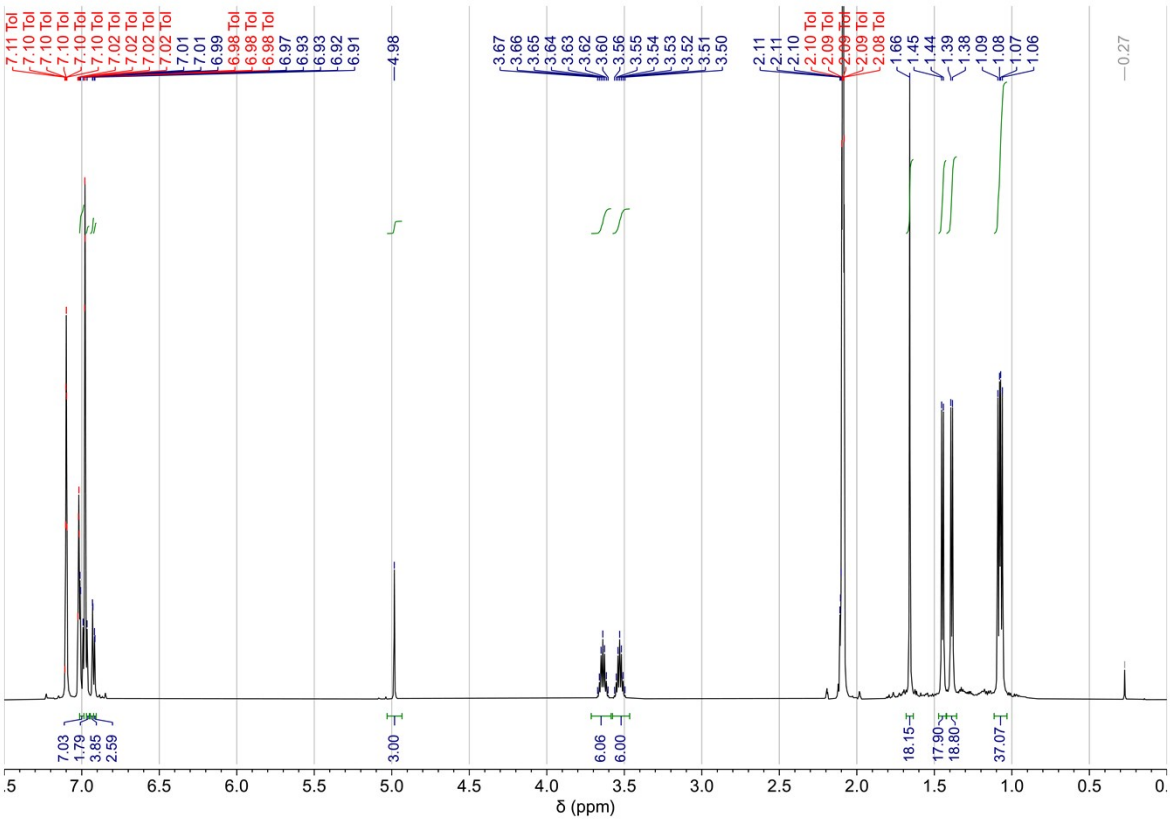

Figure S3: ^{1}H NMR spectrum (500.3 MHz, 298 K) of crystalline **2** in toluene-d_8.

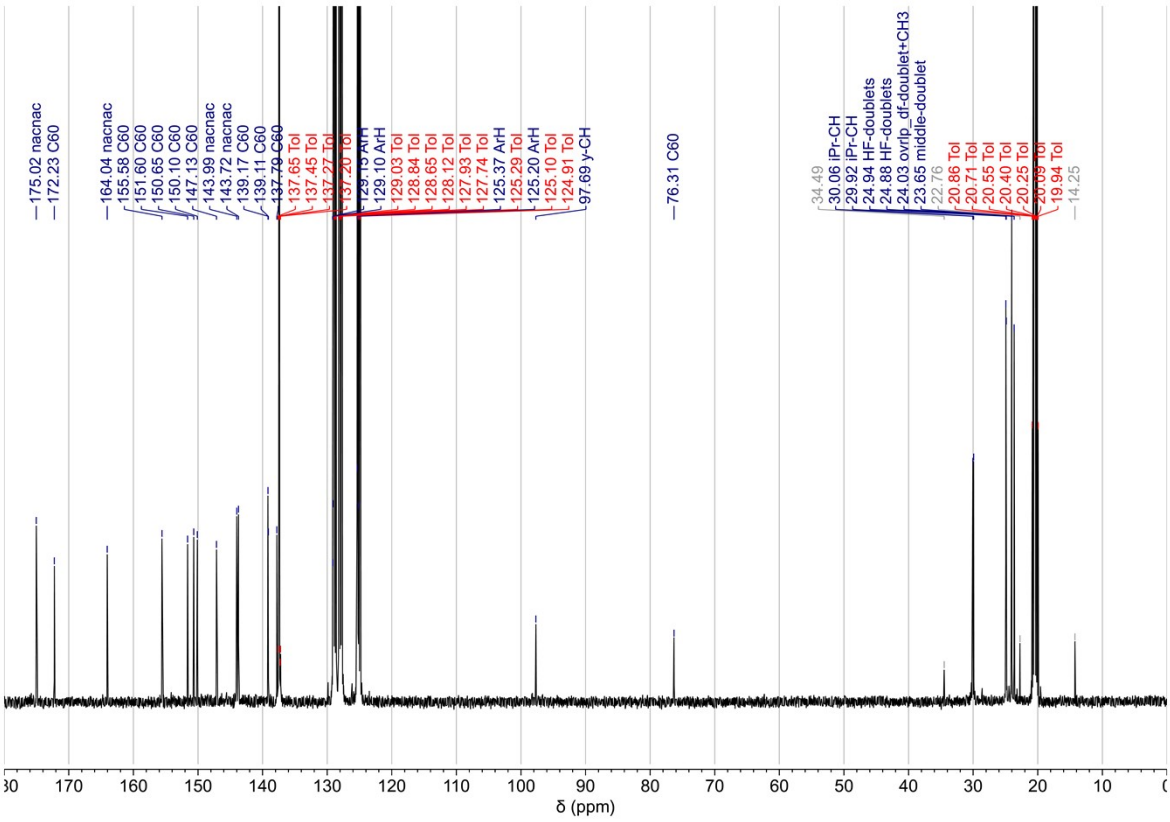

Figure S4: ^{13}C{^{1}H} NMR spectrum (125.8 MHz, 298 K) of **2** in toluene-d_8.

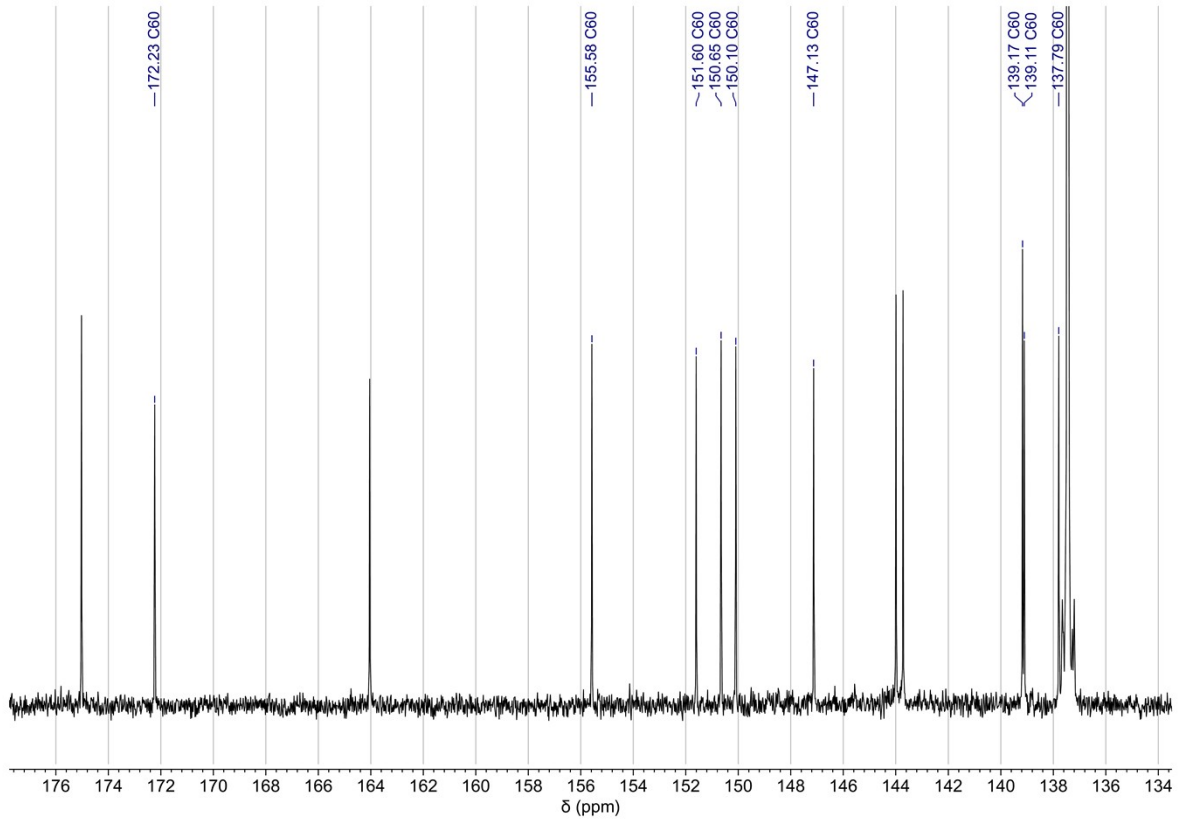

Figure S5: Expansion of the aromatic region of $^{13}C\{^{1}H\}$ NMR spectrum (500.3 MHz, 298 K) of **2** in toluene-d_8, with resonances associated to the C_{60} unit in the structure indicated.

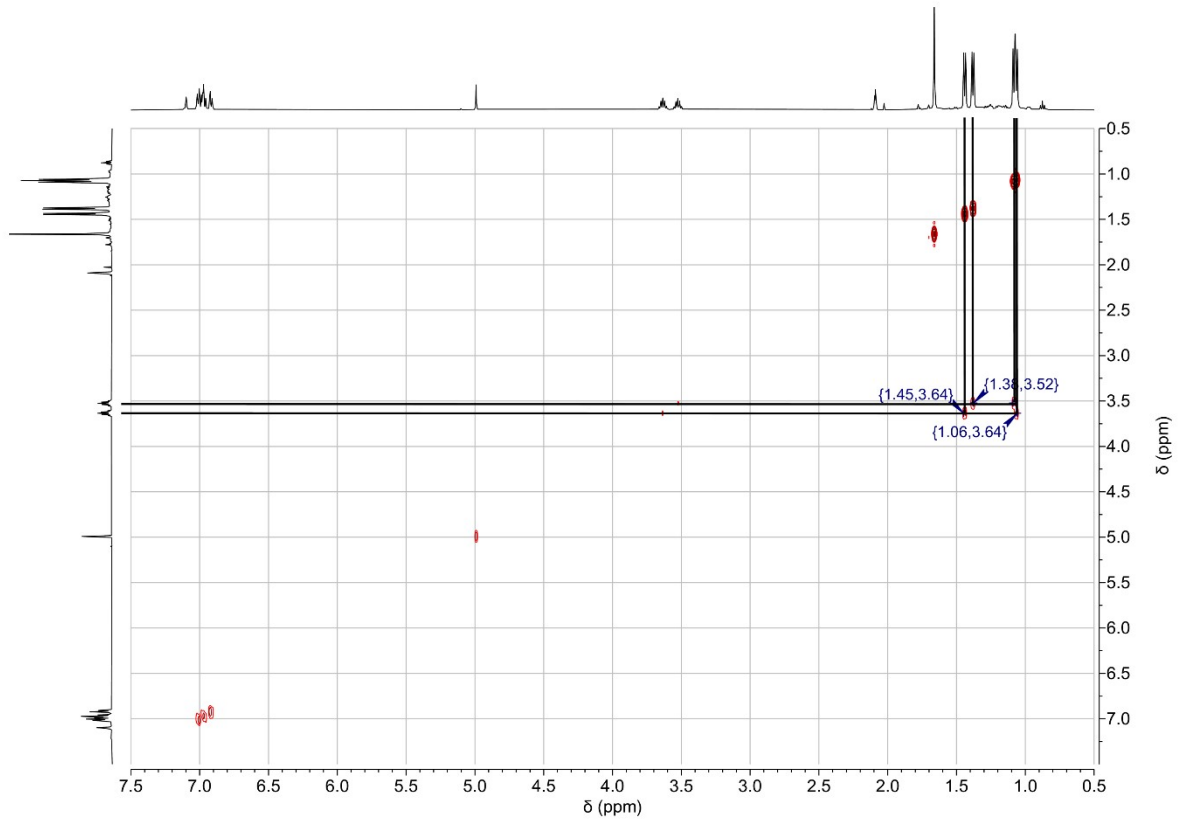

Figure S6: ^{1}H-^{1}H COSY spectrum of **2** in toluene-d_8.

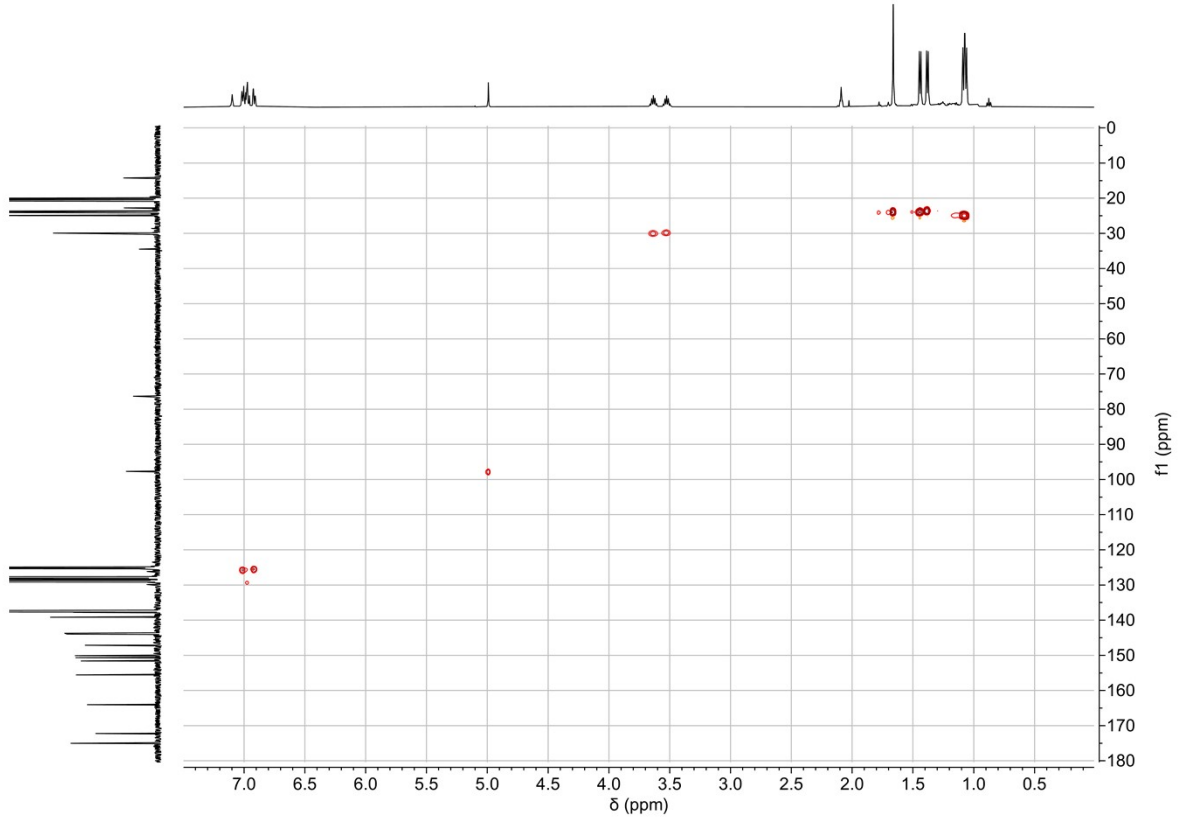

Figure S7: ^{1}H-^{13}C HSQC spectrum of **2** in toluene-d_8.

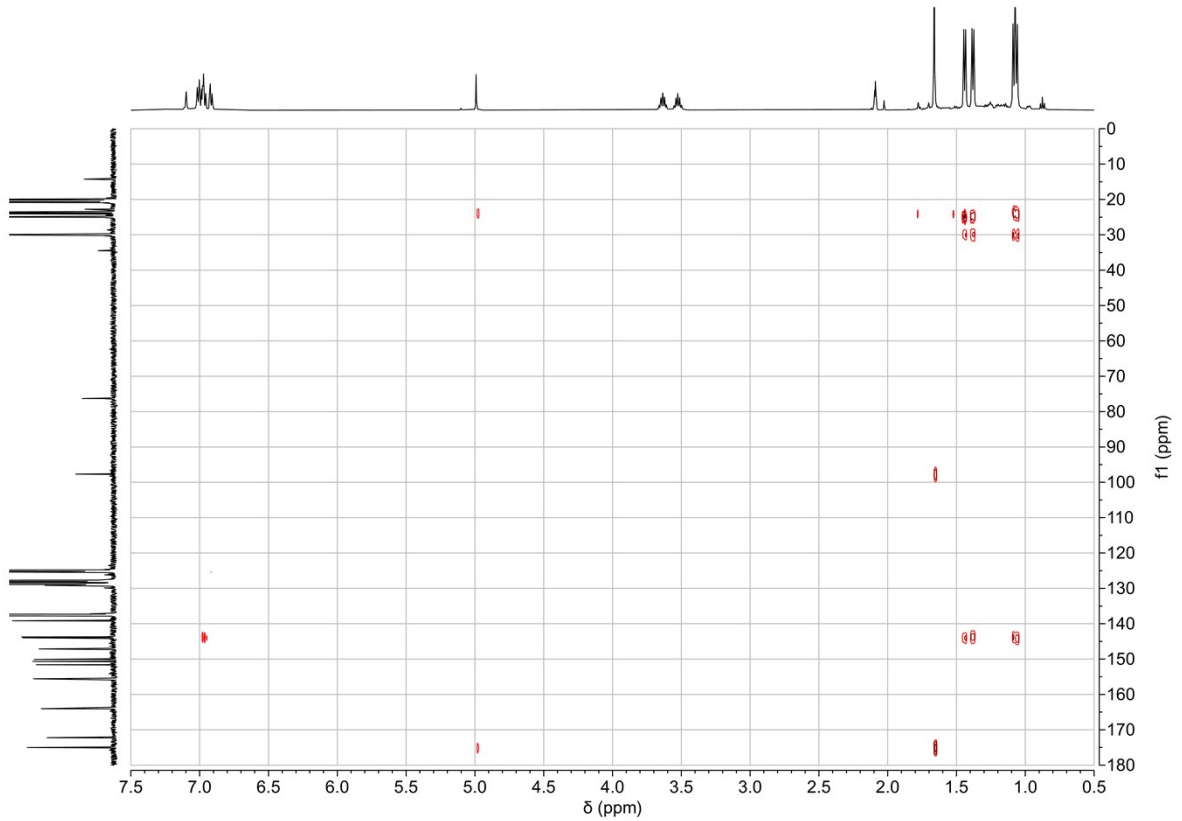

Figure S8: ^{1}H-^{13}C HMBC spectrum of **2** in toluene-d_8.

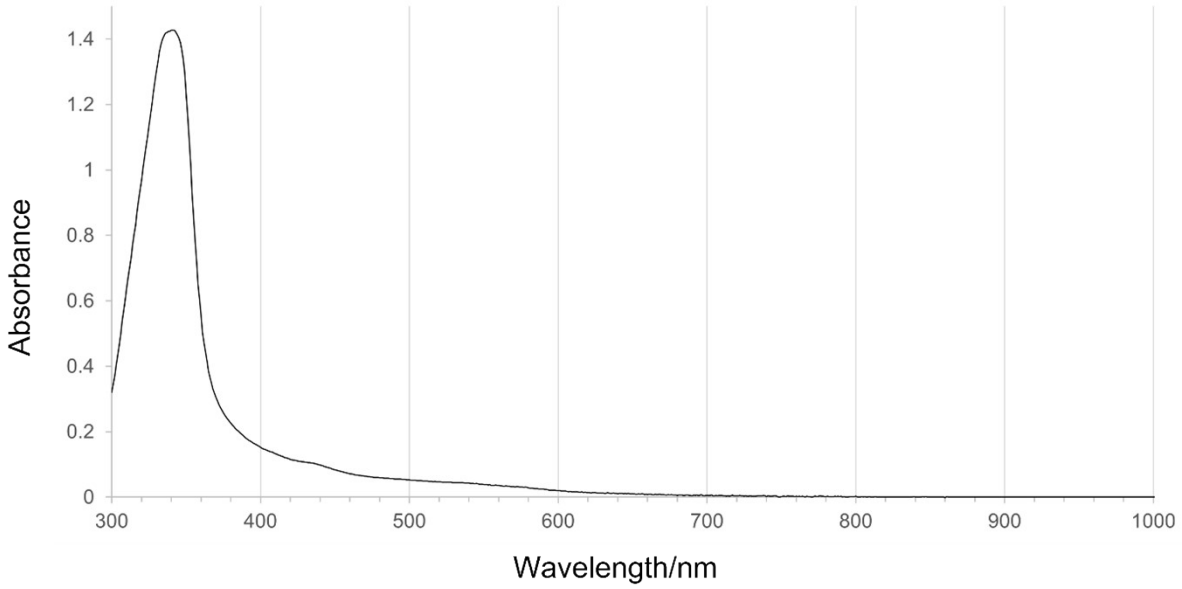

Figure S9: UV/vis spectra of **2** in toluene (*ca.* 0.42 μmol dm^{-3}). The absorbance maximum is at ca. 341 nm. For comparison, neutral C_{60} shows a maximum at 328 nm under similar conditions.[4]

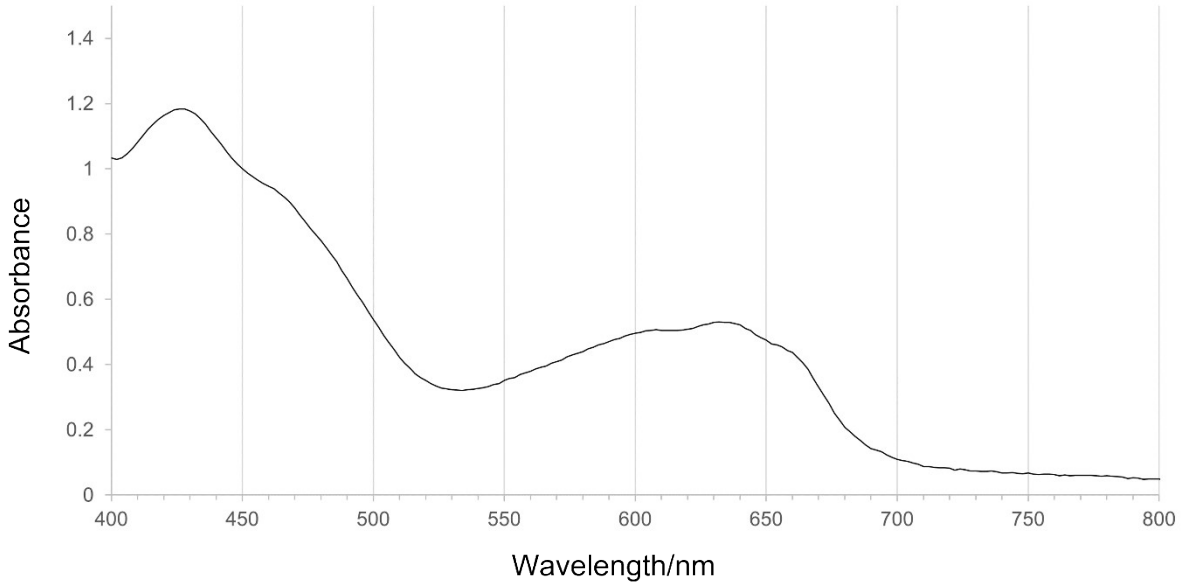

Figure S10: UV/vis spectrum of a concentrated toluene solution (*ca.* 0.2 mmol dm^{-3}) of **2**. A large maxima is observed in the UV region (300–400 nm) and when diluting to accommodate analysis of this maxima, a colour change of the solution from green to orange occurs, indicating hydrolysis.

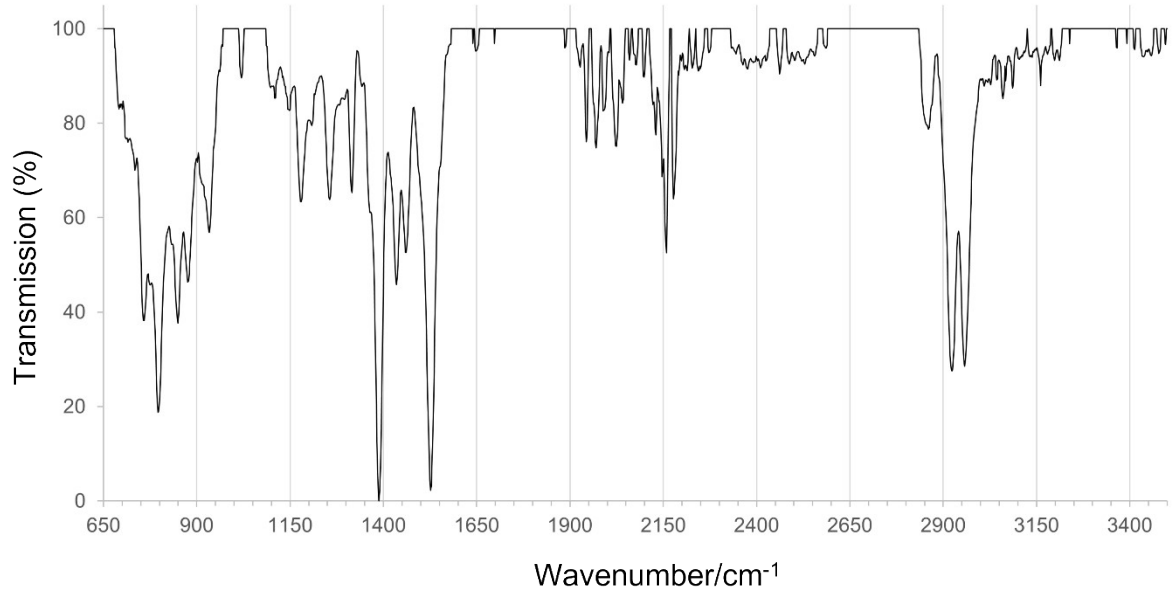

Figure S11: IR spectrum of **2**.

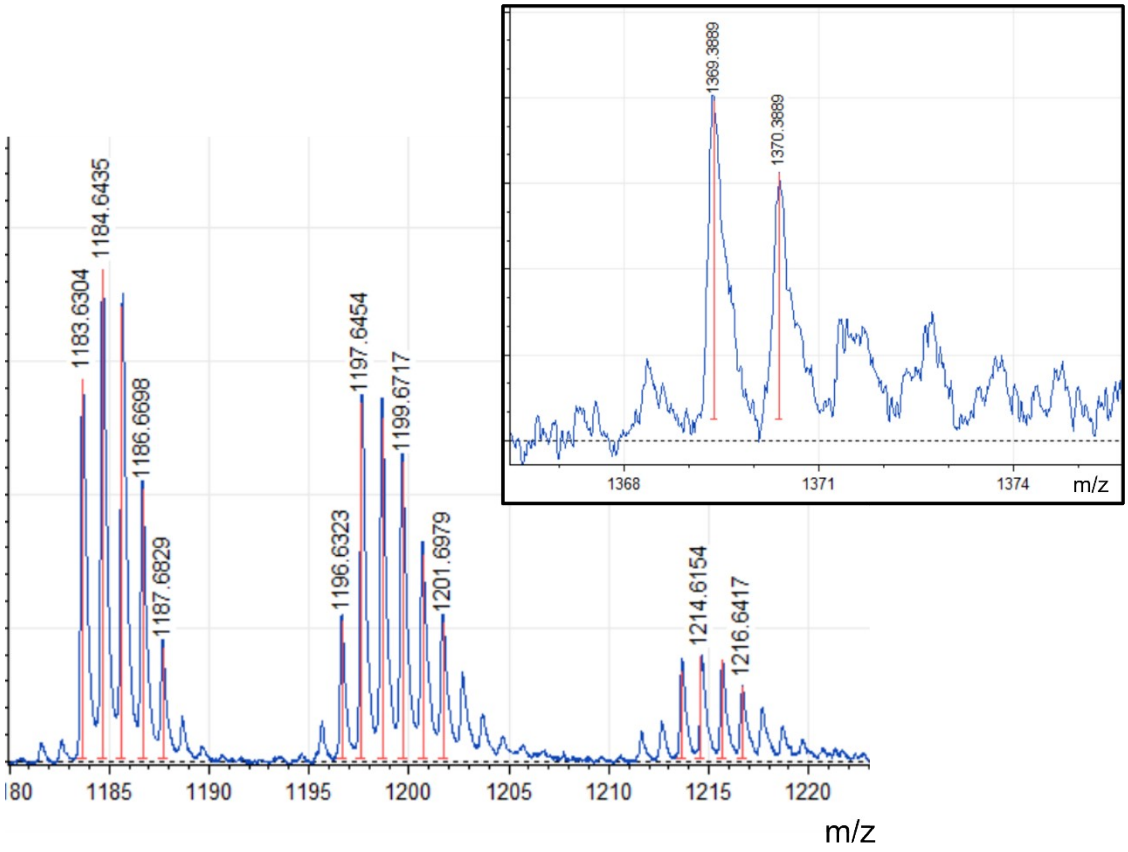

Figure S12: High molecular weight isotope patterns from the MALDI-TOF mass spectrum of **2**.

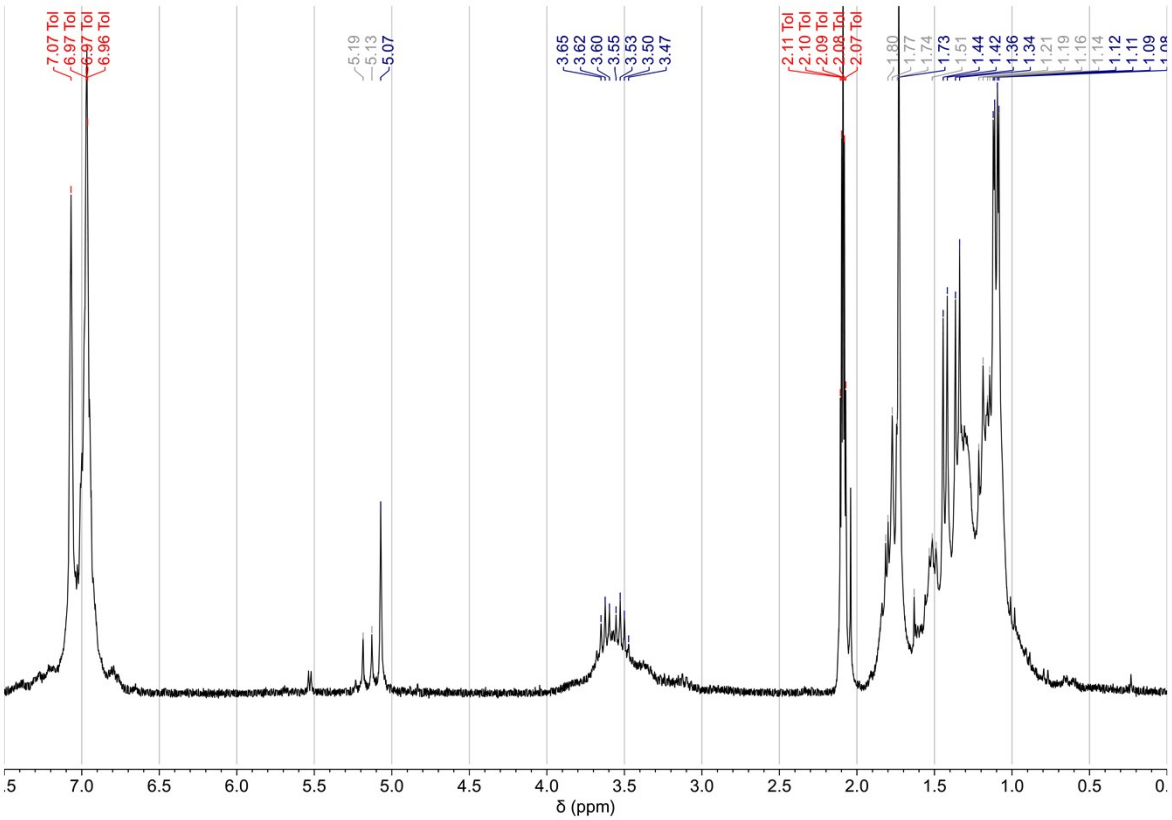

Figure S13: Variable temperature ^{1}H NMR spectrum (250.1 MHz, 353 K) of **2** in toluene-d_8 obtained after *ca.* 20 minutes at 80°C.

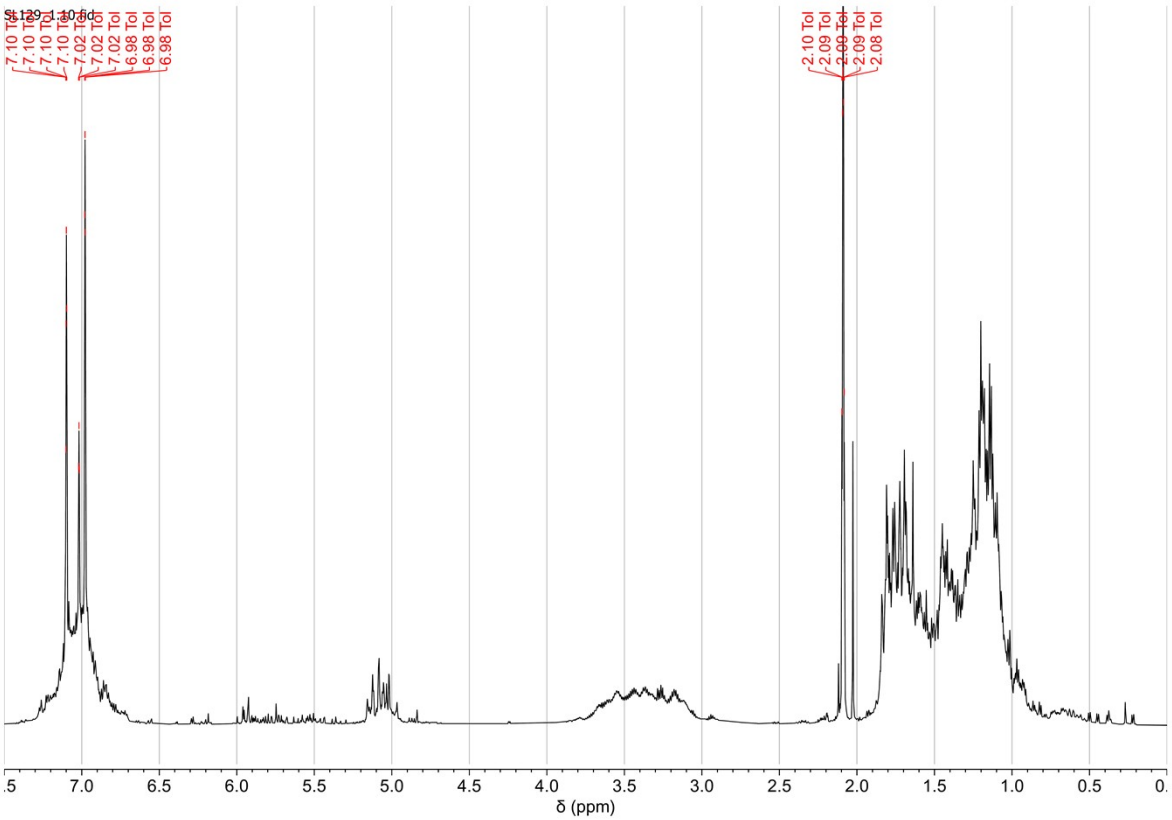

Figure S14: ^{1}H NMR spectrum (600.1 MHz, 298 K) of **2** in toluene-d_8 after variable temperature measurements (i.e. thermal decomposition of **2**), i.e., after two hours at 80°C.

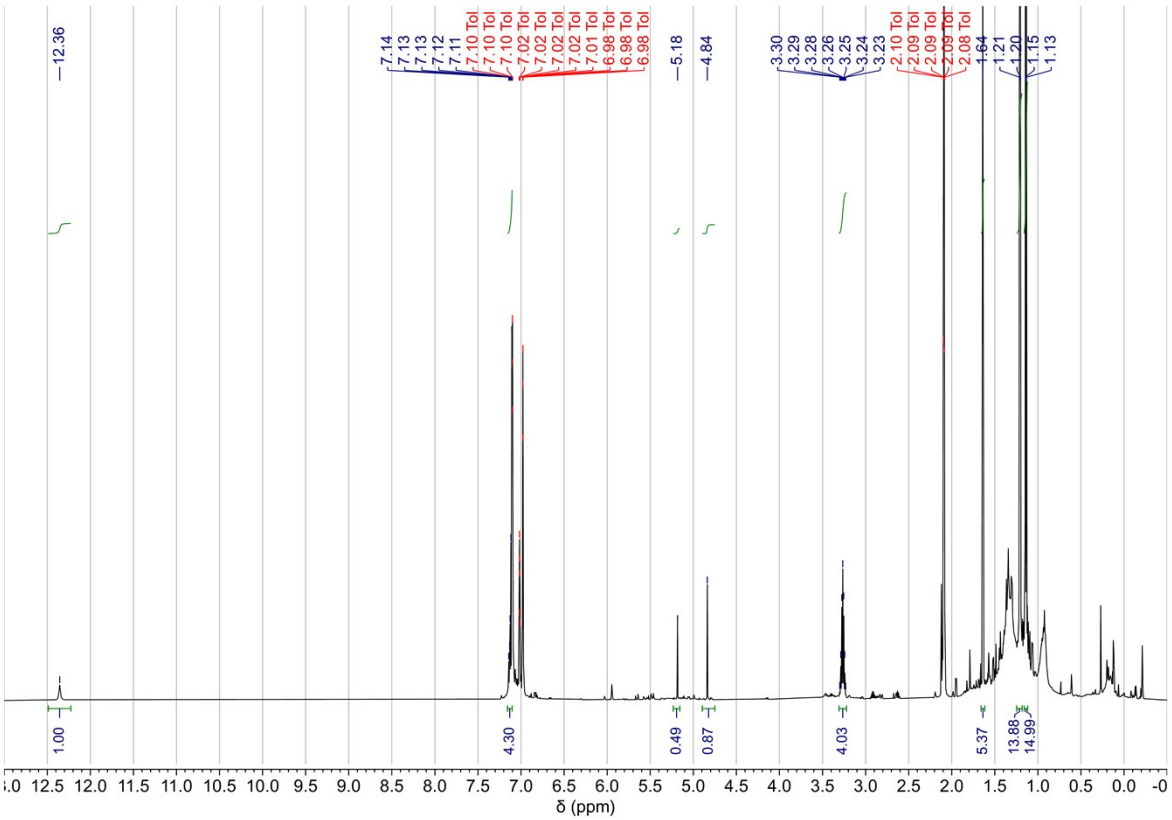

Figure S15: ^{1}H NMR spectrum (600.1 MHz, 298 K) of the crude reaction mixture of the hydrolysis product of **2**, in toluene-d_8. The predominant resonances, except δ = 5.18 ppm ($C_{60}H_6$) correspond to ^{Dipp}nacnacH ligand.[9]

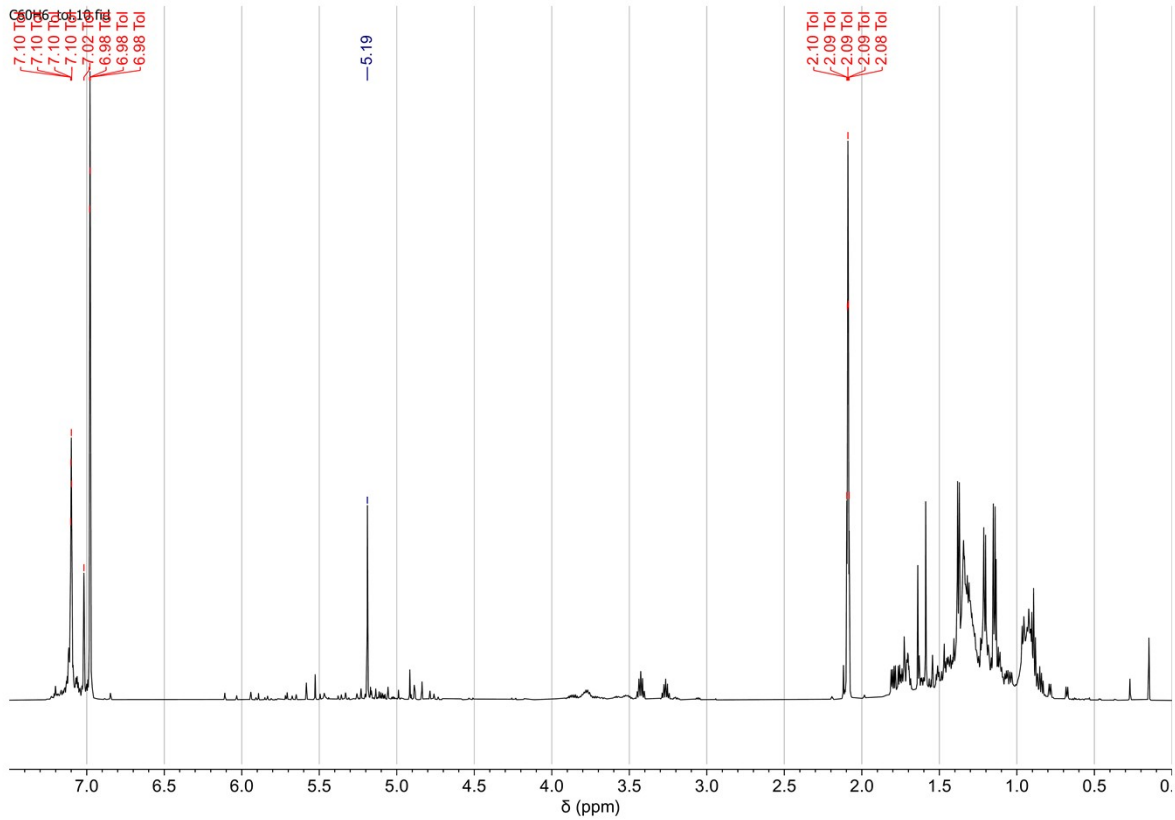

Figure S16: ^{1}H NMR spectrum (600.1 MHz, 298 K) of washed $C_{60}H_6$ following hydrolysis of **2**, in toluene-d_8.

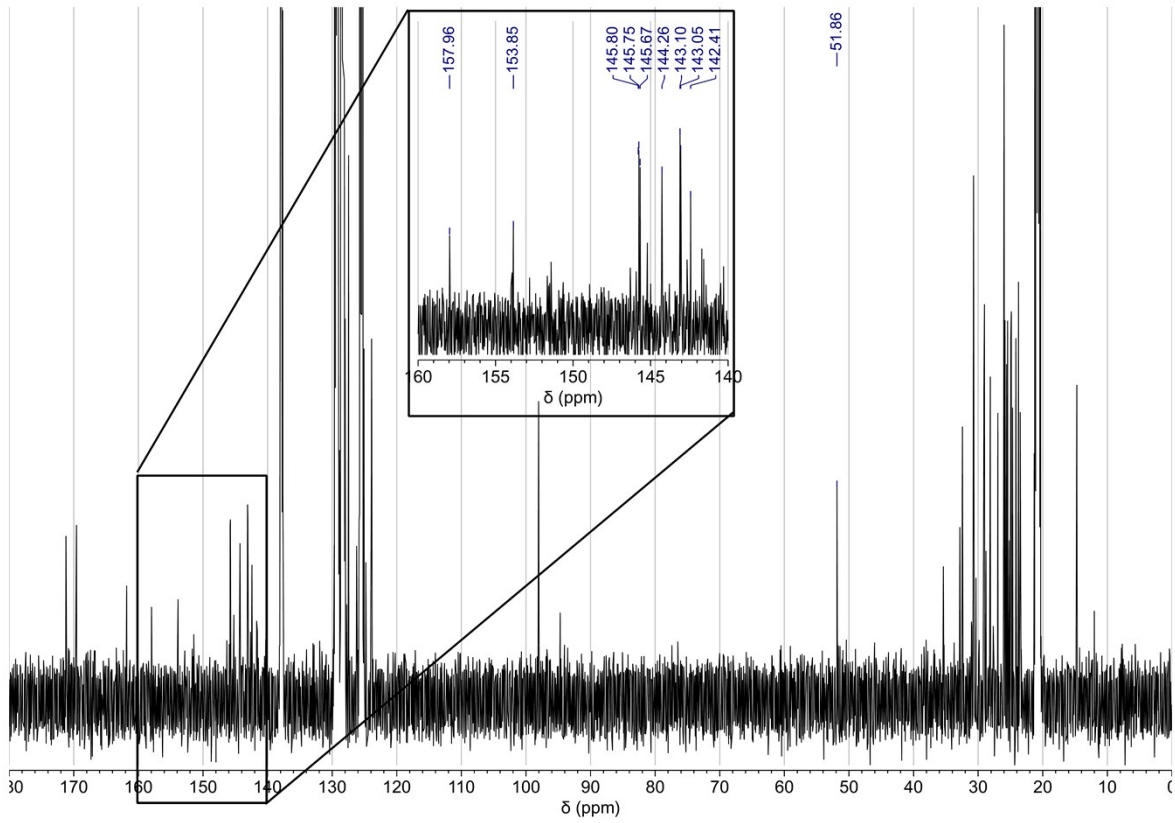

Figure S17: ^{13}C{^{1}H} NMR spectrum (600.1 MHz, 298 K) of washed $C_{60}H_6$ following hydrolysis of **2**, in toluene-d_8.

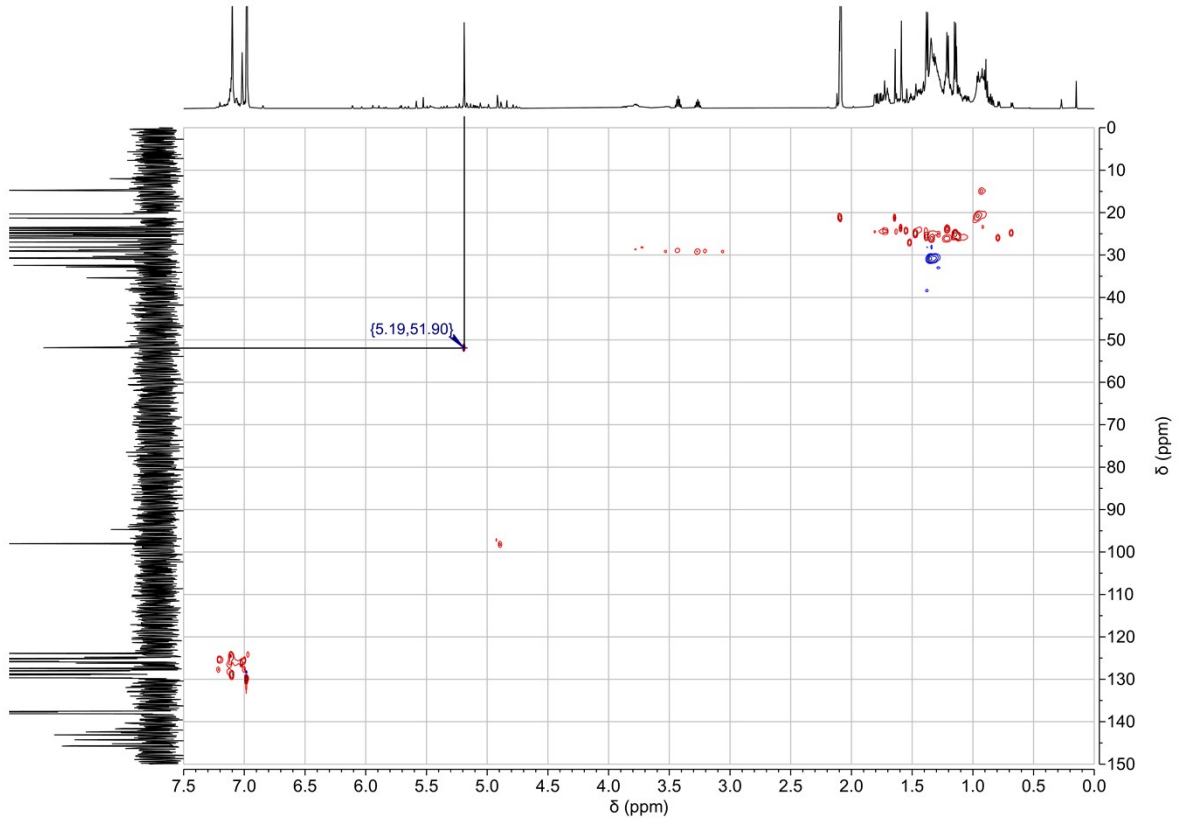

Figure S18: ^{1}H-^{13}C HSQC NMR spectrum of washed $C_{60}H_6$ following hydrolysis of **2**, in toluene-d_8.

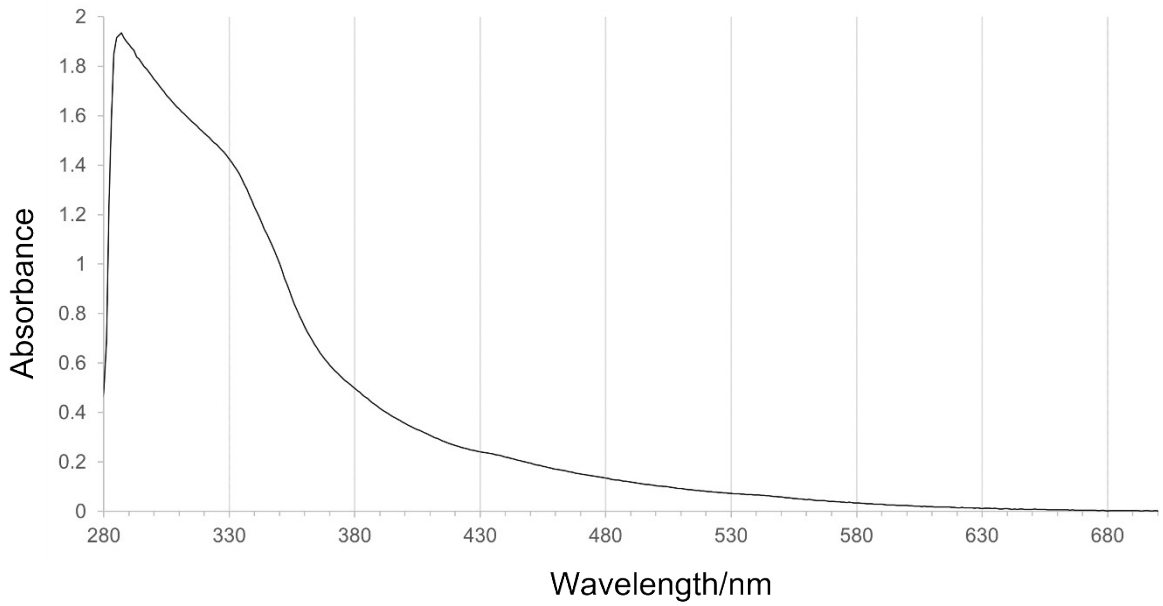

Figure S19: UV/vis spectrum of $C_{60}H_6$ (hydrolysis reaction product) in toluene; maxima [nm]: 287, 334sh. The assignment agrees well with a previously recorded UV/vis spectrum of $C_{60}H_6$.[8]

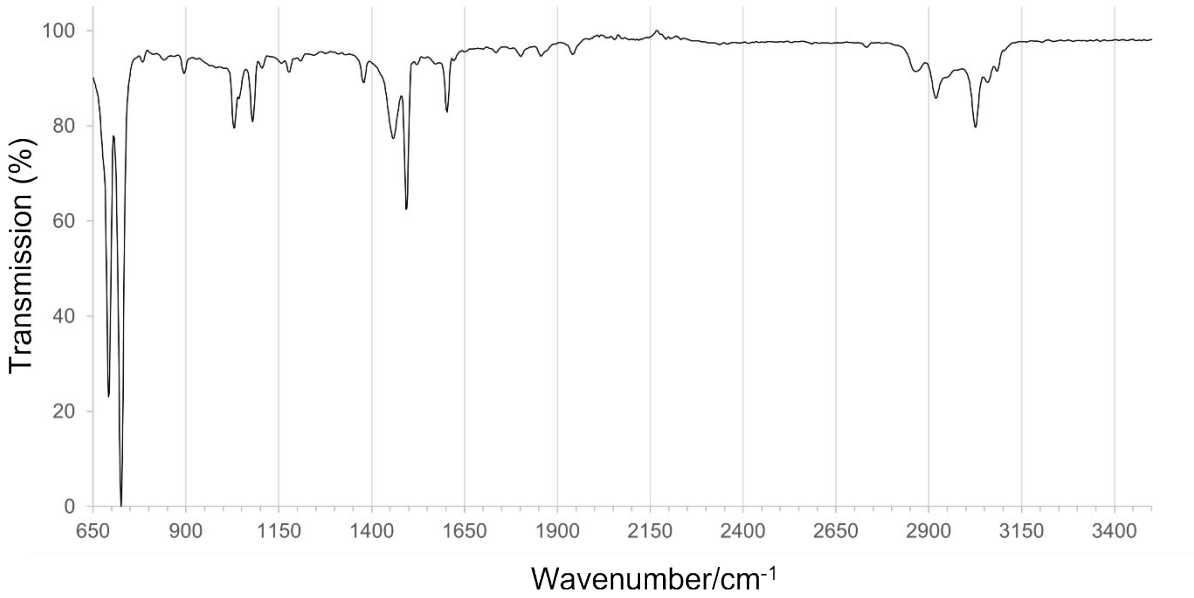

Figure S20: IR spectrum of $C_{60}H_6$ (hydrolysis reaction product). ν_{max}/cm^{-1} 3026m (C-H), 2920m (C-H), 2872br (C-H), 1602w, 1494s (C=C), 1459m (C=C), 1381w, 1079m (C-C), 1030m (C-C), 724vs, 693vs.

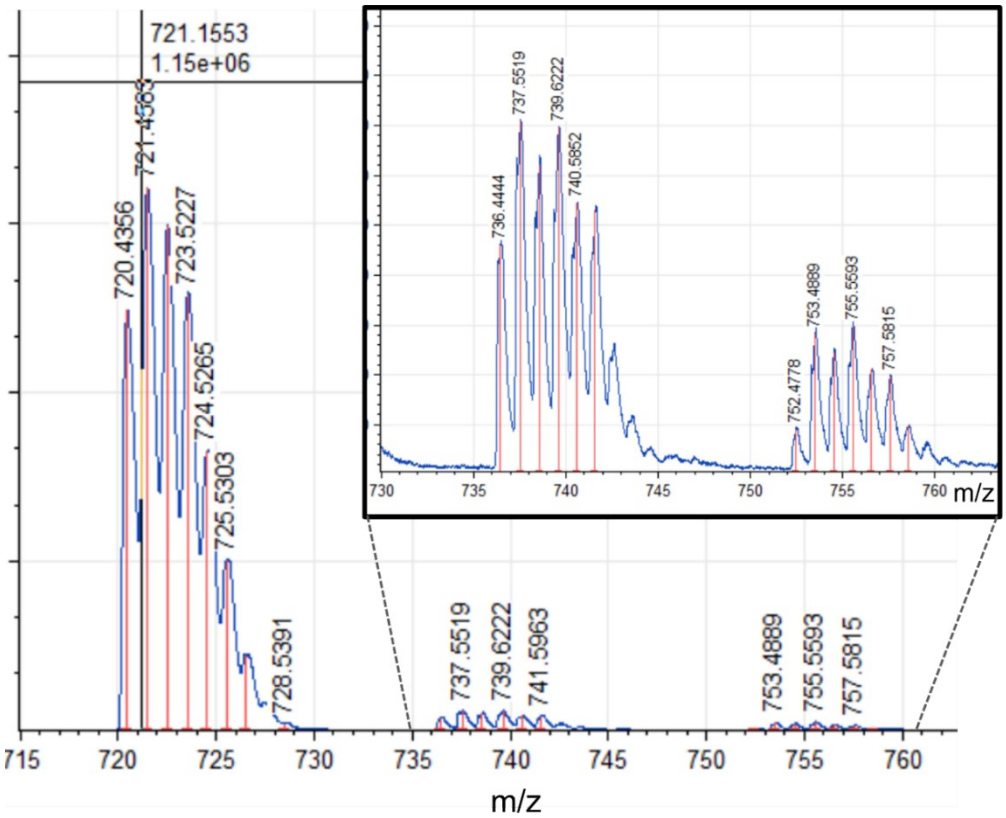

Figure S21: MALDI-TOF mass spectrum of **2**. Hydrolysis occurred during the preparation of the samples. The isotope pattern at 720-728 m/z compares well with previous reports of $C_{60}H_6$.[8]

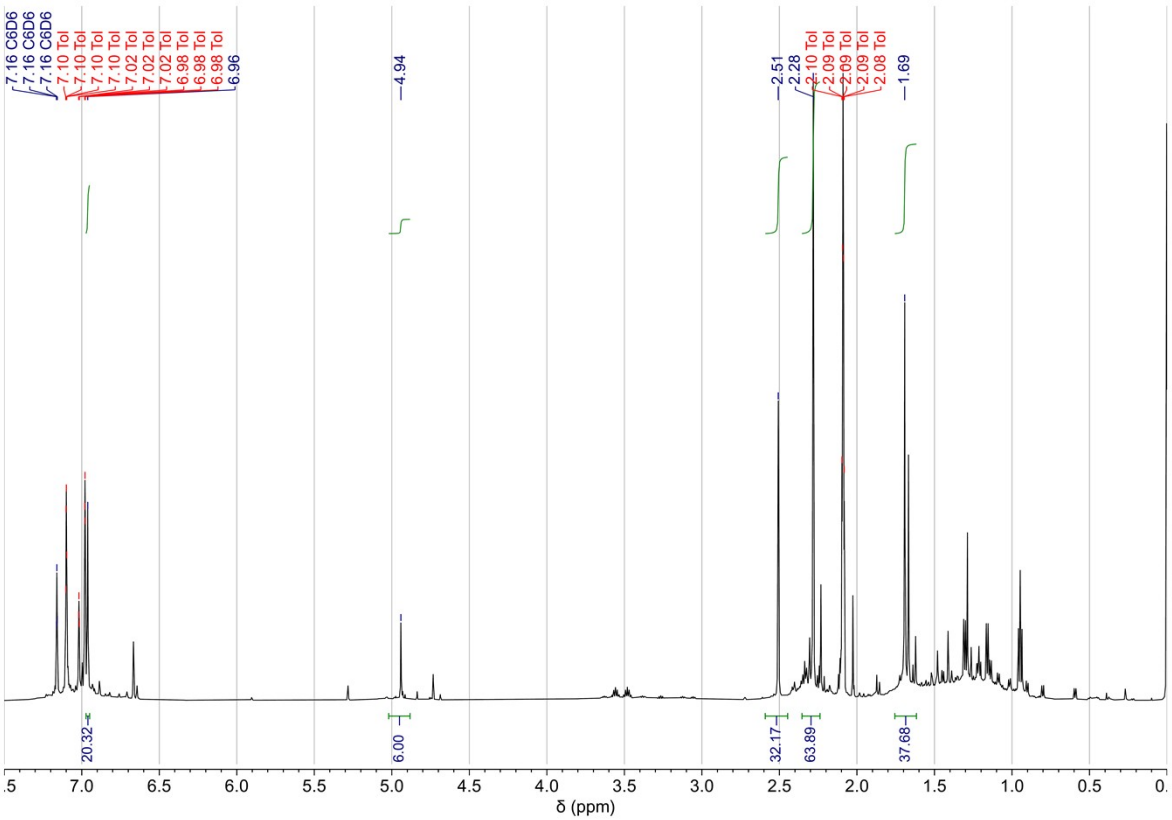

Figure S22: ^{1}H NMR spectrum (600.1 MHz, 298 K) of the crude reaction mixture after reaction of **2** with [{(^{Mes}nacnac)Mg}$_2$], in toluene-d_8.

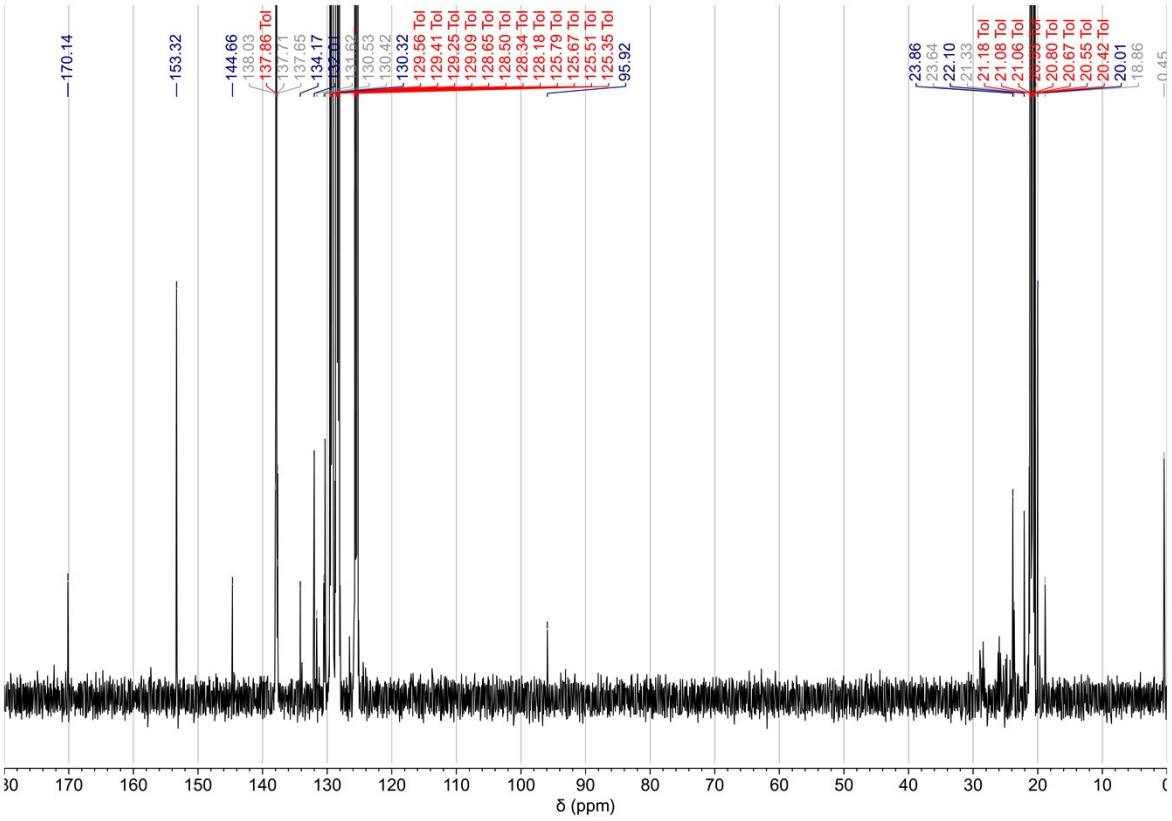

Figure S23: ^{13}C{^{1}H} NMR spectrum (150.9 MHz, 298 K) of the crude reaction mixture after reaction of **2** with [{(^{Mes}nacnac)Mg}$_2$], in toluene-d_8.

3. Single-crystal X-ray diffraction analysis

The single-crystal X-ray structure determination on **2** was carried out at 110 K on a Bruker Venture D8 diffractometer equipped with Cu Kα generator, area detector and liquid nitrogen cryostat. Crystals of **2** were embedded in an inert oil (Krytox®, GPL107) and a suitable one was selected under an optical microscope and mounted on a CryoLoop (Hampton Research, type: 20 micron and 0.2-0.3 mm diameter), with the CryoLoop fixed on a tiny glass needle. The structure was solved by direct methods and refined by full-matrix least squares techniques against F_0^2 using SHELXS[10] and SHELXL2014[11] implemented in the WINGX v2013.3 suite.[12] All non-hydrogen atoms were refined anisotropically, while hydrogen atoms were added in idealized positions, allowed to ride on the parent carbon atoms and treated isotropically with U(H) = 1.2Ueq(C) for methylene, methine and aromatic hydrogens and U(H) = 1.5Ueq(C) for methyl hydrogens. The unit cell contains 684 Å^3 (5.1%) of solvent-accessible voids.[13]

The command SQUEEZE of the PLATON program[14] was applied to give an electron count per unit cell of 183. Considering that one toluene molecule possess 50 electrons one calculates its total electron count per unit cell (Z = 4, C2/c) with 200 electrons. That is in fair coincidence with the SQUEEZE calculated value of 184 electrons per unit cell.

The asymmetric unit comprises two further toluene molecules of which one with the atoms C75-C81/C75'-C81' was refined with full occupancy but disordered over two positions with occupation factors of 0.9/0.1. The second one with the atoms C82-C88/C82'-C88' was refined with half occupancy and disordered over two position with occupation factors of 0.35/0.15.

CCDC-2253113 contains the supplementary crystallographic data for this paper. These data can be obtained free of charge from The Cambridge Crystallographic Data Centre via www.ccdc.cam.ac.uk/data_request/cif.

Table S1. Selected crystal and structural refinement data for **2**.

Empirical formula	$C_{168}H_{147}Al_3N_6$ [+ solvent]
Formula weight g/mol	2330.85
Crystal system	monoclinic
Space group	C2/c
a/Å	31.118(4)
b/Å	18.864(3)
c/Å	22.833(3)
α/°	90
β/°	91.874(5)
γ/°	90
Volume/Å^3	1
Z	4
ρ_{calc} g/cm^3	1.156
μ/mm^{-1}	0.684
F(000)	4944
Crystal size/mm3	0.3 x 0.2 x 0.1
2*Θ* range for data collection/°	2.739 to 71.043
Index ranges	$-38 \leq h \leq 38$, $-23 \leq k \leq 23$, $-27 \leq l \leq 27$
Reflections collected	261315
Independent reflections	12937
Data/restraints/parameters	12937/20/807
Goodness-of-fit on F2	1.040
Final *R* indexes [$I \geq 2\sigma(I)$]	R_1 = 0.0692, wR_2 = 0.2105
Final *R* indexes [all data]	R_1 = 0.0704, wR_2 = 0.2118
Largest diff. peak/hole / e Å-3	1.522 / -0.467

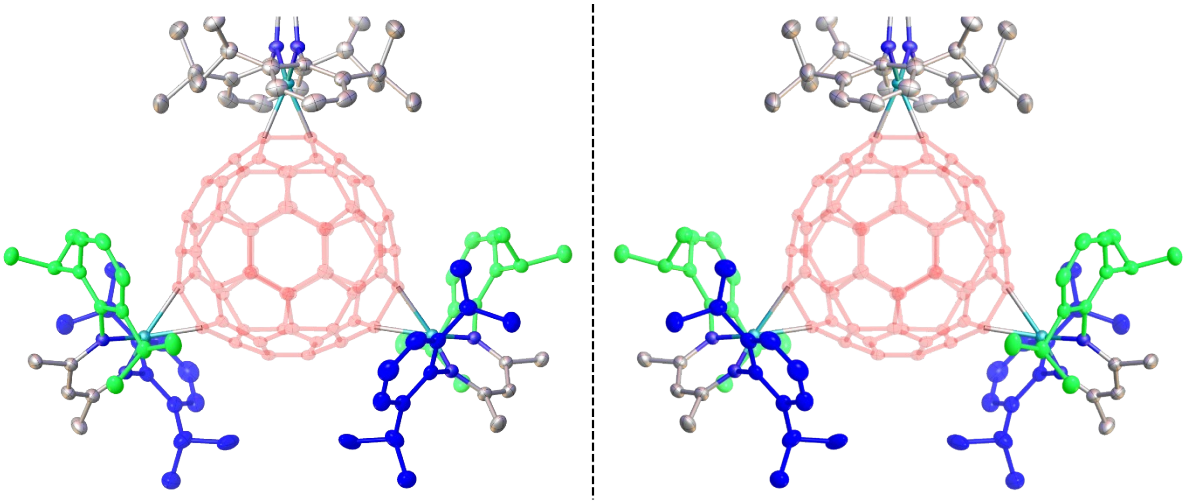

Figure S24: Helical chirality in **2**.

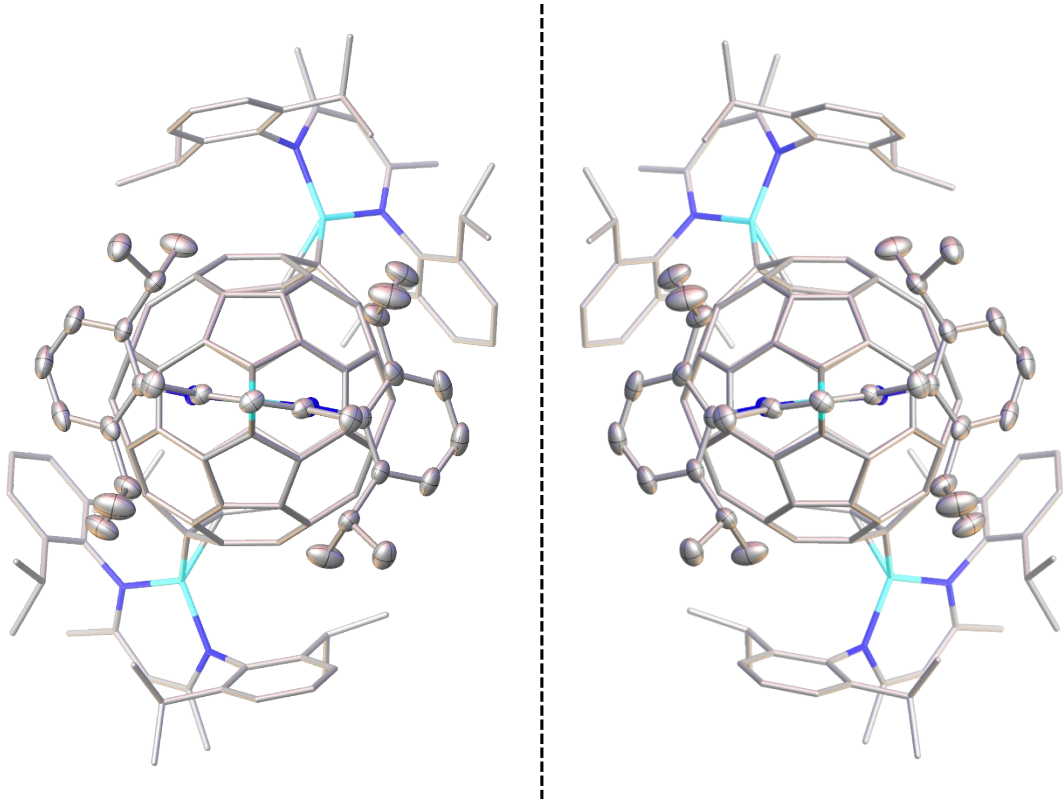

Figure S25: Asymmetry in the structure of **2**.

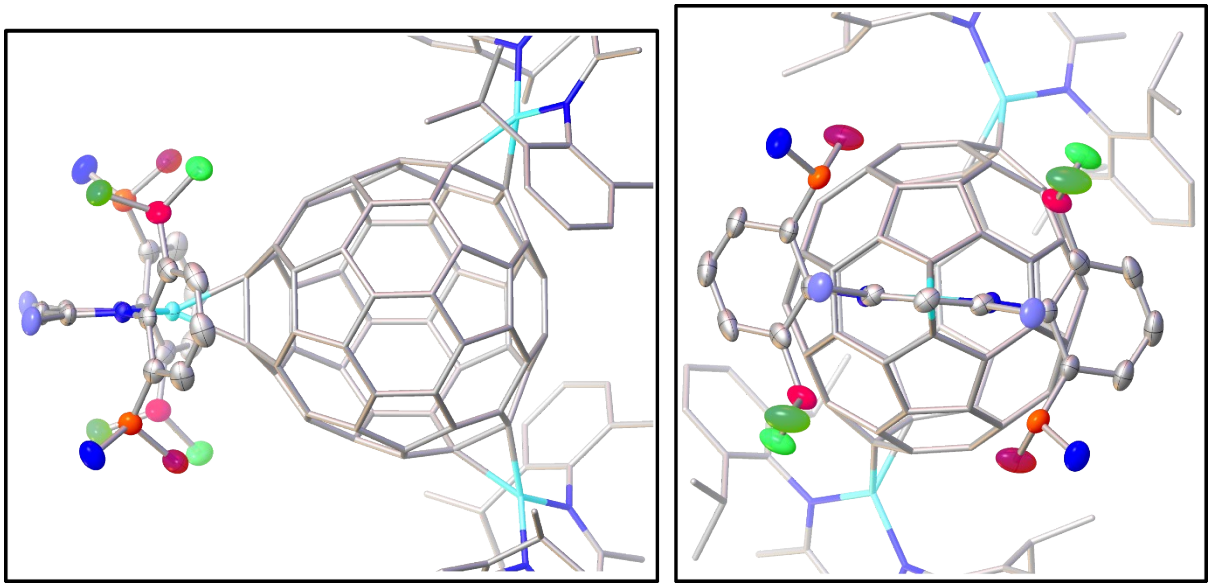

Figure S26: Anisotropy of the ^{i}Pr groups in **2**.

4. Computational Details

All geometry optimizations and frequency calculations were performed with the Gaussian16 program package.[15] Starting from crystallographic data, geometry optimization was performed using the BP86 functional,[16,17] def2-SVP basis sets,[18] and the D3 version of Grimme's dispersion correction with the Becke-Johnson damping (to account for dispersion effects)[19]. In addition, the protocol previously applied for an N-heterocyclic carbene C60 adduct has been used for comparison.[20] This includes the B3LYP functional[21] in conjunction with 6-31G(d,p)[22] (also denoted as 6-31G**) basis sets. Please note that Grimme's dispersion correction with the Becke-Johnson damping (GD3BJ)[19] was applied in deviation from the original protocol. In addition, a functional denoted B3LYP10 based on B3LYP, comprising 10 % of exact-exchange, 58.5 % of non-local B88[22] exchange and the LYP[21b] correlation, was used. As shown in a recent combined experimental and computational investigation, the latter functional provides an unambiguous description of structural and of electronic ground state properties for dinuclear aluminium complexes.[23] For all calculations, the absence of imaginary frequencies confirmed stationary points as minima

Table S2. Selected bond lengths of **2** along with the respective computed values.

	Experimental	BP86(GD3BJ)/def2SVP	B3LYP(GD3BJ)/ 6-31G(d,p)	B3LYP10(GD3BJ)/ 6-31G(d,p)
Al–C	1.9551(3) - 1.9779(2) Å	1.978 - 1.979 Å	1.959 - 1.960 Å	1.963 - 1.964 Å
Al–N	1.8633(19) - 1.8697(19) Å	1.886 - 1.887 Å	1.886 - 1.887 Å	1.885 - Å
C–C	1.63908(19) - 1.64899(17)	1.616 - 1.617 Å	1.642 - 1.643 Å	1.637 - 1.638 Å
λ_{max}	341, 426 and 632 nm	565 and 739 nm	406 and 583 nm	489 and 647 nm

In here, both the B3LYP(GD3BJ)/6-31G(d,p) as well as the B3LYP10(GD3BJ)/6-31G(d,p) protocol provide optimized ground-state structures whose values are closer to the values obtained from single-crystal X-ray diffraction, Table S2. The BP86(GD3BJ)/def2SVP combination overestimates the Al–C and Al–N bonds and underestimates the C–C bonds.

Subsequently, excited state properties such as excitation energies, oscillator strengths and electronic characters were calculated at the time-dependent DFT (TDDFT) level of theory. Therefore, the 50 lowest singlet excited states were calculated within the respective equilibrium structure. Thereby, the same functional/basis set combinations were applied as for the preceding geometry optimization. Effects of interaction with a solvent (toluene: ε = 2.374, n = 1.497) were taken into account on the ground and excited states properties by the

solute electron density (SMD) variant of the integral equation formalism of the polarizable continuum model.[24] The D3 version of Grimme's dispersion correction with the Becke-Johnson damping (to account for dispersion effects)[19].

The XYZ coordinates of the geometry optimized structures are given in the separate XYZ file.

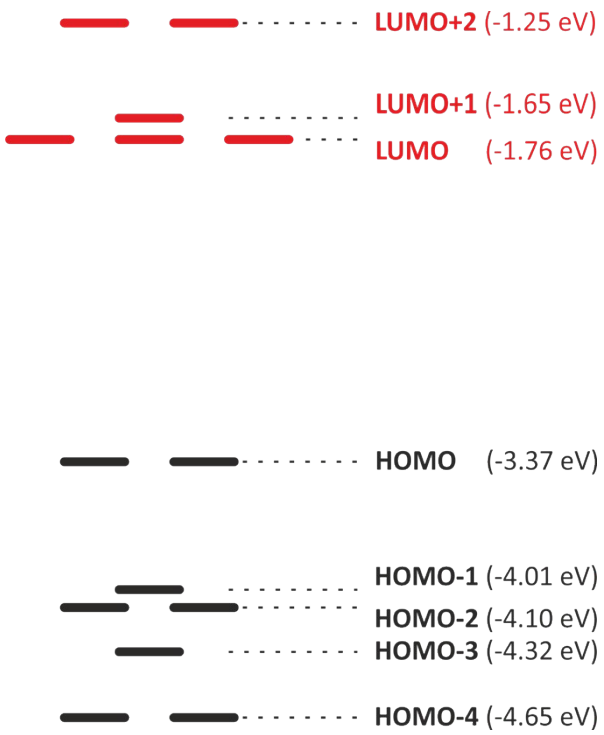

Figure S27: Molecular orbital diagram of **2** obtained at the B3LYP10(GD3BJ)/6-31G(d,p)/(SMD(toluene) level of theory.

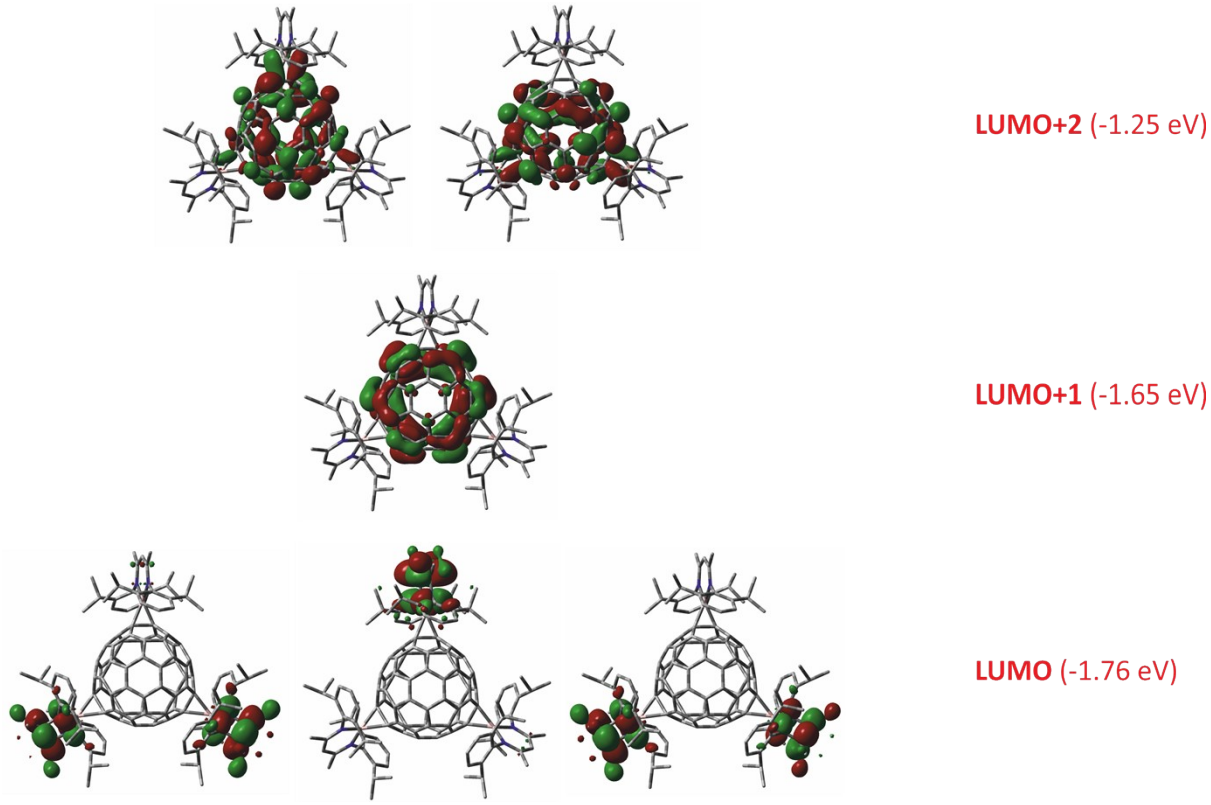

Figure S28: LUMO to LUMO+2 of **2** obtained at the B3LYP10(GD3BJ)/6-31G(d,p)/(SMD(toluene) level of theory.

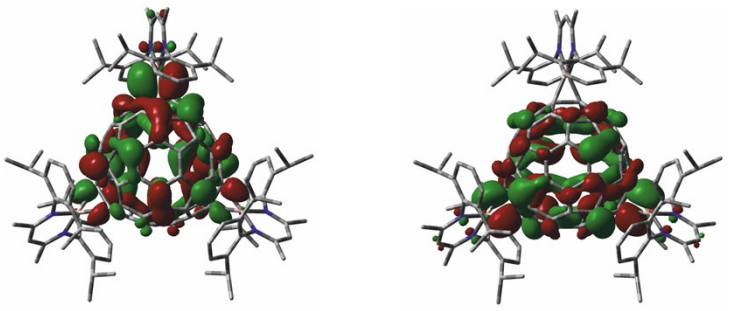

HOMO (-3.37 eV)

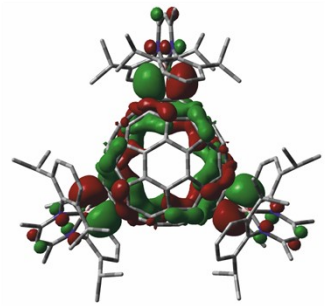

HOMO-1 (-4.01 eV)

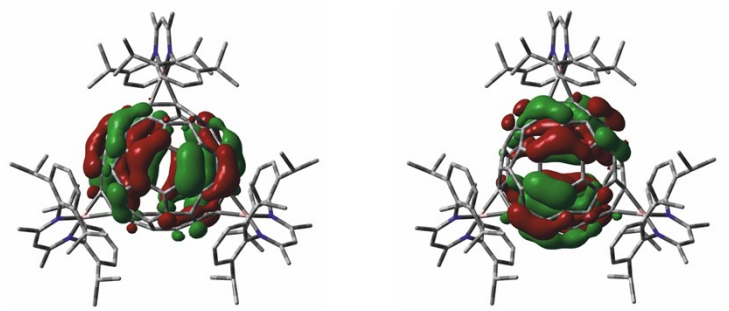

HOMO-2 (-4.10 eV)

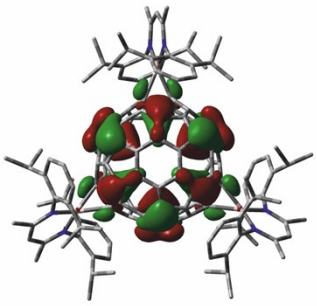

HOMO-3 (-4.32 eV)

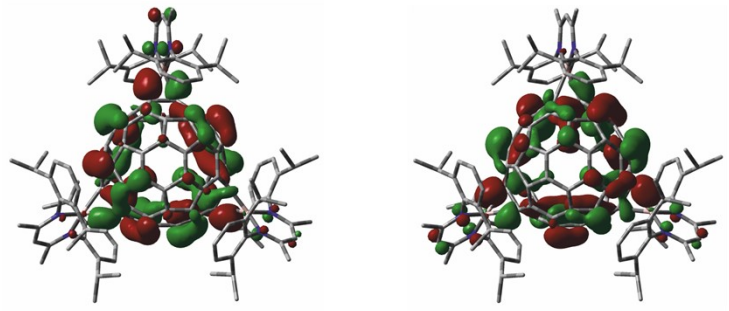

HOMO-4 (-4.65 eV)

Figure S29: HOMO to HOMO-4 (isovalue 0.02 au) of **2** obtained at the B3LYP10(GD3BJ)/6-31G(d,p)/(SMD(toluene) level of theory.

5. References

1) O. Kysliak, H. Görls and R. Kretschmer, *Dalton Trans.*, 2020, **49**, 6377-6383.
2) a) S. J. Bonyhady, C. Jones, S. Nembenna, A. Stasch, A. J. Edwards and G. J. McIntyre, *Chem. Eur. J.*, 2010, **16**, 938–955; b) J. Hicks, M. Juckel, A. Paparo, D. Dange and C. Jones, *Organometallics*, 2018, **37**, 4810−4813.
3) S. R. Lawrence, C. A. Ohlin, D. B. Cordes, A. M. Z. Slawin and A. Stasch, *Chem. Sci.*, 2019, **10**, 10755–10764.
4) H. Ajie, M. M. Alvarez, S. J. Anz, R. D. Beck, F. Diederich, K. Fostiropoulos, D. R. Huffman, W. Krätschmer, Y. Rubin, K. E. Schriver, D. Sensharma and R. L. Whetten, *J. Phys. Chem.*, 1990, **94**, 8630–8633.
5) a) T. Chu, Y. Boyko, I. Korobkov and G. I. Nikonov, *Organometallics*, 2015, **34**, 5363−5365; b) M R. Crimmin, M. J. Butler and A. J. P. White, *Chem. Commun.*, 2015, **51**, 15994−15996.
6) T. Chu, I. Korobkov and G. I. Nikonov, *J. Am. Chem. Soc.*, 2014, **136**, 9195−9202.
7) C. Cui, S. Köpke, R. Herbst-Irmer, H. W. Roesky, Mathias M. Noltemeyer, H. -G. Schmidt and B. Wrackmeyer, *J. Am. Chem. Soc.*, 2001, **123**, 9091−9098.
8) M. S. Meier, B. R. Weedon and H. P. Spielmann, *J. Am. Chem. Soc.*, 1996, **118**, 11682–11683.
9) D. Adhikari, B. L. Tran, F. J. Zuno-Cruz, G. Sanchez Cabrera and D. J. Mindiola, in *Inorganic Syntheses*, ed T. B. Rauchfuss, John Wiley & Sons, Inc., 2010, **35**, ch. 3. pp. 8-13.
10) G. M. Sheldrick, *Acta Cryst.*, 2015, **C71**, 3–8.
11) G. M. Sheldrick, *Acta Cryst.*, 2015, **C71**, 3–8.
12) L. J. Farrugia, *J. Appl. Cryst.*, 2012, **45**, 849–854.
13) A. L. Spek, *Acta Cryst.*, 2009, **D65**, 148–155.
14) PLATON – A Multipurpose Crystallographic Tool – © 1980-2015, A. L. Spek, version 70515.
15) Gaussian 16, Revision C.01, M. J. Frisch, G. W. Trucks, H. B. Schlegel, G. E. Scuseria, M. A. Robb, J. R. Cheeseman, G. Scalmani, V. Barone, G. A. Petersson, H. Nakatsuji, X. Li, M. Caricato, A. V. Marenich, J. Bloino, B. G. Janesko, R. Gomperts, B. Mennucci, H. P. Hratchian, J. V. Ortiz, A. F. Izmaylov, J. L. Sonnenberg, D. Williams-Young, F. Ding, F. Lipparini, F. Egidi, J. Goings, B. Peng, A. Petrone, T. Henderson, D. Ranasinghe, V. G. Zakrzewski, J. Gao, N. Rega, G. Zheng, W. Liang, M. Hada, M. Ehara, K. Toyota, R. Fukuda, J. Hasegawa, M. Ishida, T. Nakajima, Y. Honda, O. Kitao, H. Nakai, T. Vreven, K. Throssell, J. A. Montgomery, Jr., J. E. Peralta, F. Ogliaro, M. J. Bearpark, J. J. Heyd, E. N. Brothers, K. N. Kudin, V. N. Staroverov, T. A. Keith, R. Kobayashi, J. Normand, K. Raghavachari, A. P. Rendell, J. C. Burant, S. S. Iyengar, J. Tomasi, M. Cossi, J. M. Millam, M. Klene, C. Adamo, R. Cammi, J. W. Ochterski, R. L. Martin, K. Morokuma, O. Farkas, J. B. Foresman and D. J. Fox, Gaussian, Inc., Wallingford CT, 2016.
16) A. D. Becke, *Phys. Rev. A*, 1988, **38**, 3098–3100.
17) J. P. Perdew, *Phys. Rev. B*, 1986, **33**, 8822–8824.
18) F. Weigend and R. Ahlrichs, *Phys. Chem. Chem. Phys*., 2005, **7**, 3297–3305.
19) S. Grimme, S. Ehrlich and L. Goerigk, *J. Comp. Chem.*, 2011, **32**, 1456–1465.
20) H. Li, C. Risko, J. H. Seo, C. Campbell, G. Wu, J.-L. Brédas and G. C. Bazan, *J. Am. Chem. Soc.*, 2011, **133**, 12410–12413.
21) a) A. D. Becke, *J. Chem. Phys.*, 1993, *98*, 5648-5652; b) C. Lee, W. Yang, and R. G. Parr, *Phys. Rev. B*, 1988, **37**, 785-789.
22) a) R. Ditchfield, W. J. Hehre, J. A. Pople, *J. Chem. Phys.*, 1971, **54**, 724-728; b) W. J. Hehre, R. Ditchfield, J. A. Pople, *J. Chem. Phys.*, 1972, **56**, 2257-2261; c) P. C. Hariharan, J. A. Pople, *Theor. Chim. Acta*, 1973, **28**, 213-222; d) M. M. Francl, W. J. Pietro, W. J. Hehre, J. S. Binkley, M. S. Gordon, D. J. DeFrees, J. A. Pople, *J. Chem.*

Phys., 1982, **77**, 3654-3665; e) M. S. Gordon, J. S. Binkley, J. A. Pople, W. J. Pietro, W. J. Hehre, *J. Am. Chem. Soc*., 1982, **104**, 2797-2803.

23) F. L. Portwich, Y. Carstensen, A. Dasgupta, S. Kupfer, R. Wyrwa, H. Gorls, C. Eggeling, B. Dietzek, S. Grafe, M. Wachtler, and R. Kretschmer, *Angew. Chem., Int. Ed*. 2022, **61**, e202117499.

24) a) B. Mennucci, C. Cappelli, C. A. Guido, R. Cammi, and J. Tomasi, *J. Phys. Chem. A* 2009, **113**, 3009; b) A. V. Marenich, C. J. Cramer, and D. G. Truhlar, *J. Phys. Chem. B* 2009, **113**, 6378.